Expanding GABAergic Neuronal Diversity in PSC-Derived Disease Models

Ruiqi Hu[1, 2, 3, 4, 12], Linda L. Boshans[1, 2, 3, 4, 12], Yiran Tao[1, 2, 3, 4], Bohan Zhu[5], Junglong Li[6,7], Xindi Li[6, 7], Rui Dang[8], Marianna Liang[1, 2, 3, 4, 9], Peiwen Cai[5], Mark Youssef[1, 2, 3, 4], Gizem Inak[1, 2, 3, 4], Yingnan Song[5, 10, 11], Xuran Wang[5, 10, 11], Alexander M Tsankov [5], Joseph D. Buxbaum[5, 10,11], Peng Jiang[8], Zhiping P. Pang[6, 7], Sai Ma[5], Nan Yang[1,2,3,4,13]

1. Nash Family Department of Neuroscience, Friedman Brain Institute, Icahn School of Medicine at Mount Sinai, New York, NY, 10029, USA
2. Alper Center for Neurodevelopment and Regeneration, Icahn School of Medicine at Mount Sinai, New York, NY 10029, USA.
3. Institute for Regenerative Medicine, Icahn School of Medicine at Mount Sinai, New York, NY 10029, USA.
4. Black Family Stem Cell Institute, Icahn School of Medicine at Mount Sinai, New York, NY, 10029, USA
5. Department of Genetics and Genomic Sciences, Icahn School of Medicine at Mount Sinai, New York, NY 10029, USA.
6. Center for NeuroMetabolism, The Child Health Institute of New Jersey, Rutgers Robert Wood Johnson Medical School, New Brunswick, NJ 08901, USA
7. Department of Neuroscience and Cell Biology, Rutgers Robert Wood Johnson Medical School, New Brunswick, NJ 08901, USA
8. Department of Cell Biology and Neuroscience, Rutgers University, New Brunswick, Piscataway, NJ 08854, USA
9. Department of Neurology, Icahn School of Medicine at Mount Sinai, 1425 Madison Avenue, New York, NY 10029, USA.
10. Seaver Autism Center for Research and Treatment, Icahn School of Medicine at Mount Sinai, New York, NY 10029, USA.
11. Department of Psychiatry, Icahn School of Medicine at Mount Sinai, New York, NY 10029, USA
12. These authors contributed equally
13. Lead contact

*Correspondence: sai.ma@mssm.edu (S.M.); nan.yang1@mssm.edu (N.Y.)

SUMMARY

GABAergic interneurons comprise diverse molecular and functional subtypes that contribute to neural circuit assembly and are implicated in a range of neurodevelopmental and neuropsychiatric disorders. Traditional approaches for differentiating human pluripotent stem cells (PSCs) into neurons often face challenges such as incomplete neural differentiation, prolonged culture periods, and variability across PSC lines, which can constrain their application in disease modeling. To address these limitations, we developed a strategy that combines inducible expression of the transcription factors (TFs) ASCL1 and DLX2 with dual-SMAD and WNT inhibition to efficiently drive differentiation of human PSCs into diverse, region-specific GABAergic neuronal types. Using single-cell sequencing, we characterized the cellular heterogeneity of GABAergic induced neurons (iNs) generated with the patterning factors (patterned iNs) and those derived solely with TFs (PSC-derived iNs), revealing distinct interneuron subtype compositions and the regulatory programs that govern their fate specification. Patterned iNs exhibited gene expression features corresponding to multiple brain regions, particularly the ganglionic eminence (GE) and neocortex, whereas GABAergic PSC-derived iNs predominantly resembled hypothalamic and thalamic neurons. Both iN types were enriched for genes relevant to neurodevelopmental and psychiatric disorders, with patterned iNs more specifically linked to neural lineage genes, highlighting their utility for disease modeling. We further applied this protocol to investigate the impact of a recurrent ADNP syndrome-associated mutation (p.Tyr719*) on GABAergic neuron differentiation, revealing that this mutation disrupts GABAergic fate specification and synaptic transmission. Overall, this study expands the toolkit for disease modeling by demonstrating the complementary advantages of GABAergic PSC-derived iNs and patterned iNs in representing distinct GABAergic neuron subtypes, brain regions, and disease contexts. Together, these approaches provide a flexible platform for investigating molecular and cellular mechanisms relevant to neurodevelopmental and neuropsychiatric disorders.

INTRODUCTION

Inhibitory GABAergic (γ-aminobutyric acid, GABA) neurons comprise a highly diverse class of cells defined by distinct molecular identities and are essential for the organization of neural circuits.[1,2] Forebrain interneurons are generated in transient progenitor domains in the ventral telencephalon, known as the ganglionic eminences (GE), including the medial, caudal, and lateral ganglionic eminences (MGE, CGE, and LGE). These progenitor domains generate interneuron populations with diverse molecular and functional properties.[3,4] MGE-derived interneurons predominantly mature into parvalbumin-expressing (PV; PVALB) or somatostatin-expressing (SST/SOM) cortical interneurons,[5-9] whereas CGE generates vasoactive intestinal peptide (VIP)-expressing interneurons and populations expressing calretinin (CR; CALB1), LAMP5, and CCK.[6,10-12] More recent studies indicate that dorsal LGE-derived interneurons also contribute to cortical inhibitory populations, particularly in frontal regions and deep white matter, and are marked by MEIS2, FOXP2, and PAX6,[13,14] highlighting the multiple developmental origins underlying cortical interneuron diversity.

Perturbations in interneuron specification and function have been implicated in autism spectrum disorder (ASD), epilepsy, schizophrenia, Alzheimer's disease (AD), and numerous other neurodevelopmental and psychiatric disorders.[3,4,15-17] Importantly, interneurons arising from distinct developmental domains all appear to contribute to disease-relevant phenotypes, rather than any single lineage being uniquely engaged. Dysfunction of PV^+ and SST^+ interneurons, primarily derived from the MGE, has been linked to multiple neurological and neuropsychiatric disorders, including AD, ASD, schizophrenia, and epilepsy, and is often associated with disrupted inhibition, altered excitability, and imbalance in excitation/inhibition (E/I balance). Meanwhile, CGE-derived interneurons, which constitute a substantial fraction of cortical interneurons and are proportionally expanded in humans and non-human primates[18-22], have been implicated across multiple neuropsychiatric conditions[23-25], and the CGE is the primary source of tumors and lesions in tuberous sclerosis complex (TSC)[26]. Together, these findings underscore the importance of modeling GABAergic neuron diversity and of developing in vitro systems capable of generating interneurons representing a broad range of subtypes and developmental origins.

Human pluripotent stem cell (PSC)-based approaches have enabled the scalable generation of GABAergic neurons and are widely used for mechanistic and disease-focused studies. Early conventional differentiation strategies largely relied on small-molecule and morphogen-based patterning to mimic MGE development, reflecting foundational insights from

rodent studies in which MGE-derived interneurons constitute major cortical inhibitory populations. [27] Despite their utility, these approaches face several limitations, including partial induction of neural identities, protracted timelines required to generate mature neuronal cultures, limited representation of CGE- and LGE-derived subtypes, and variability in differentiation efficacy across PSC lines. In contrast to conventional paradigms, direct reprogramming of PSCs into defined cell types through forced expression of transcription factors (TFs) offers a compelling alternative. This method has been widely adopted because of its simplicity, speed, efficiency, scalability, and reproducibility. For instance, forced expression of proneural TFs such as Neurogenin-2 (NEUROG2 or NGN2) and achaete-scute complex-like 1 (ASCL1) - key regulators of neuronal fate during brain development - can rapidly induce neuronal differentiation in human PSCs. [27-31] While effective at generating neurons, TF induction alone is limited in its ability to produce the full spectrum of neuronal subtypes in the brain. Recent studies have addressed this limitation by combining TF overexpression with extrinsic patterning signals, enabling the specification of a broader range of neuronal subtypes that cannot be generated using either method alone. Notably, pre-patterning PSCs prior to NGN2 induction allows the generation of regionally specified neuronal populations, such as cortical-like or motor neurons.[32,33] Despite this progress, comparable combinatorial strategies have not been systematically explored for generating diverse and developmentally relevant GABAergic interneuron subtypes.

Previously, we demonstrated that forced expression of Ascl1 and Dlx2 efficiently induces the differentiation of human PSCs into GABAergic neurons. These GABAergic induced neurons (iNs) robustly adopt inhibitory neurotransmitter phenotypes and express subtype-specific markers, indicating the generation of potentially diverse subpopulations through this protocol.[27] We and others have shown that GABAergic iNs are valuable for investigating inhibitory synapse-specific phenotypes linked to human neurological disorders.[27,34,35] However, the characterization of GABAergic iNs has predominantly relied on electrophysiology, limited immunofluorescence markers, and bulk transcriptomic profiling. As a result, their precise subtype composition, regional correspondence to *in vivo* interneuron populations, and degree of heterogeneity remain poorly defined at single-cell resolution.

To address these outstanding issues, we demonstrate in this study that neuralization of stem cells via dual SMAD and WNT inhibition[36], followed by forced expression of ASCL1 and DLX2, effectively specifies diverse GABAergic neuronal identities that correspond to populations found in the developing forebrain. Using single-cell RNA sequencing (scRNA-seq), we

comprehensively characterize GABAergic iNs generated from small-molecule–patterned PSCs (patterned-iNs) and compare them with PSC-derived ASCL1/DLX2-iNs (PSC-iNs) and GABAergic neurons generated using small-molecule patterning alone. This comparative analysis reveals that each differentiation strategy yields a diverse array of GABAergic neuronal subtypes with composite regional identities. We also investigate the differentiation dynamics and regulatory mechanisms underlying fate specification in PSC-iNs and patterned-iNs using single-cell multiomic approaches. To further demonstrate the utility of patterned GABAergic iNs, we apply this framework to *ADNP* (activity-dependent neuroprotective protein), one of the most frequently mutated genes in syndromic autism.[37] The recurrent truncating mutation p.Tyr719* is the most common pathogenic ADNP variant identified in patients. While prior studies of ADNP have mainly focused on excitatory neuron models, the effects of ADNP mutations in human inhibitory neurons, a lineage central to E/I balance, remain poorly characterized. Using patterned GABAergic iNs, we examine how the ADNP p.Tyr719* mutation influences interneuron subtype specification and inhibitory synaptic function. Together, this work demonstrates the complementary strengths of PSC-derived and patterned GABAergic neuron models in capturing interneuron diversity across brain regions and disease contexts, providing a versatile platform for investigating molecular and cellular mechanisms underlying neurodevelopmental and neuropsychiatric disorders.

RESULTS

ASCL1 & DLX2 Induce GABAergic Neurons from Patterned Progenitors.

Direct programming leverages one or more TFs to force the establishment of a distinct transcriptional network, thereby promoting the adoption of a new cellular identity.[38,39] Previously, we reported that forced expression of ASCL1 and DLX2 in human PSCs induces rapid differentiation into GABAergic neurons (Figure 1A). This strategy has since been adopted and independently validated by multiple groups to generate human GABAergic neurons.[40,41] While these iN cells displayed core features of GABAergic neurons, including GAD1/2, DLXs, and SLC32A1 (vGAT), the homogeneity of the resulting cell population and its similarity to *in vivo* counterparts remained unclear. To address these questions, we performed single-cell RNA sequencing (scRNA-seq) to profile GABAergic PSC-iNs 42 days after ASCL1 and DLX2 expression (Figure 1A).

For comparison, we generated interneurons using a well-established directed differentiation protocol that involves dual SMAD inhibition, WNT signaling inhibition, and SHH signaling activation to specify ventral telencephalic progenitors that give rise to interneurons.[42-45] This

approach is presumed to produce GABAergic neurons similar to PSC-iNs, as evidenced by the expression of interneuron subtype markers such as SST, CR, and Calbindin (CB). [27,42] We characterized these neurons five weeks after culturing the progenitors on dissociated mouse glial cells (Figure S1A). While neurons generated using the directed differentiation method expressed GABAergic markers like *GAD1* and *DLX6-AS*, they showed minimal expression of markers associated with synaptic function, including *SLC32A1* and *SYN1*. In contrast to PSC-iNs, these neurons expressed *FOXG1*, a defining marker of forebrain identity, suggesting that they represent immature cortical interneurons (Figures S1B and S1C). The lack of FOXG1 expression in PSC-iNs indicates that they may resemble GABAergic neurons from more posterior brain regions.

These observations prompted us to test whether extrinsic patterning cues could synergize with ASCL1 and DLX2 to rapidly generate diverse inhibitory neurons associated with specific brain regions. To this end, we employed a doxycycline (DOX)-responsive piggyBac transposon system to achieve robust and controlled overexpression of ASCL1 and DLX2 in human cells. We first induced central nervous system neuroectoderm from human PSCs following an established forebrain patterning timeline, inhibiting TGF-β and BMP signaling with SB431542 and LDN193189 for 10 days, while transiently blocking WNT signaling with the tankyrase inhibitor XAV939 during the first 3 days.[46] This initial patterning phase biases cells toward a forebrain neural fate but does not by itself specify interneuron identity. Following this patterning phase, DOX was applied to induce ASCL1 and DLX2 expression, together with the γ-secretase inhibitor DAPT, to eliminate dividing progenitors and synchronize maturation.[47] Cells were then dissociated and co-cultured with mouse astrocytes to support neuronal maturation and synapse formation. To assess whether the duration of ASCL1 and DLX2 expression influences neuronal fate, DOX was withdrawn after either 3 or 7 days post-induction, generating 3D-patterned-iNs and 7D-patterned-iNs, respectively. We refer to these cells as patterned GABAergic induced neurons (patterned-iNs) to reflect the combination of brief regional patterning and transcription factor–driven fate specification. Five weeks after astrocyte co-culture, GABAergic neurons expressing MAP2 and DLX2 were detected under all experimental conditions (Figure 1A).

To gain deeper insights into the cellular composition of these cultures, we performed scRNA-seq on neurons generated under each differentiation condition and analyzed them alongside GABAergic PSC-iNs. In total, we generated transcriptomes from 12,876 cells across various differentiation strategies, including 5,314 PSC-iNs, 2,899 3D-patterned-iNs, and 4,663 7D-patterned-iNs that passed quality control (Table S1). Dimensionality reduction and

visualization using uniform manifold approximation and projection (UMAP) revealed seven molecularly distinct cell clusters that segregated by differentiation strategy (Figure S2A). Further examination of neuronal marker gene expression revealed that most cells exhibit neuronal characteristics as marked by *MAP2, STMN1,* and *SYN1* expression (Figures S2B and S2C). Most of the induced neurons (86.2%) are GABAergic, as indicated by the expression of *GAD1*, *GAD2*, *SLC32A1*, and *DLXs*. A small fraction of cells was identified as glutamatergic, based on *SLC17A6/7* expression (3D-patterned-iNs: 42/2,899; 7D-patterned-iNs: 56/4,663; PSC-iNs: 10/5,314), while only rare cells expressed markers of other neuronal lineages, including CHAT (cholinergic, 0.02%) or TH (dopaminergic, 0.06%). Notably, the proportion of cells expressing the vesicular GABA transporter *SLC32A1* was substantially lower in 3D-patterned-iNs compared with 7D-patterned-iNs (19.4% versus 50.9%). Conversely, 3D-patterned-iNs showed increased expression of genes associated with a less mature or progenitor-like state, including *SOX2* (7.0% versus 0.94% in 7D-patterned-iNs). These data suggest that 3 days of ASCL1 and DLX2 expression are insufficient to fully drive small-molecule patterned progenitor-like cells into a mature neuronal state. Together, our data demonstrate that the duration of TF expression, in combination with extrinsic patterning cues, critically influences neuronal maturation and supports the synergistic use of TFs and small molecules to generate GABAergic neurons from human PSCs.

Molecularly Diverse GABAergic Neurons Generated by Distinct Differentiation Strategies.

To further investigate heterogeneity among induced GABAergic neurons (iGABAs), we extracted *SLC32A1*-expressing neurons, comprising 4,086 PSC-iGABAs, 574 3D-patterned-iGABAs, and 1,915 7D-patterned-iGABAs. Unsupervised clustering based on gene expression identified five major molecular clusters, with clear separations between clusters depending on the differentiation method used (Figure 1B). As expected, all clusters consistently expressed canonical markers of the GABAergic lineage while generally devoid of markers indicative of other neuronal lineages (Figures 1C and S3A). Consistent with our previously reported immunofluorescence analysis, these clusters showed variable enrichment for inhibitory neuron subtype markers, including *SST*, *CALB1*, *CALB2*, *VIP,* and *NPY* (Figures 1C, 1D, and S3A).[27] When examining the differentially expressed TFs across these clusters, we found *FOXG1* expressed in patterned-iGABAs (clusters 3 and 4). The gene expression signature of 7D-patterned-iGABAs (cluster 2) reflected spatial origins and subtypes associated with the CGE and LGE, marked by *NR2F2* (*COUP-TFII*), *PAX6*, and *ISL1*.[13,48,49] *ISL1* was also strongly expressed in cluster 0, which consisted of PSC-iGABAs, whereas PSC-iGABAs in cluster 1

robustly expressed *FOXA2* and *NKX2-2*, markers associated with hypothalamic inhibitory neurons.[50,51] In addition to TFs, we identified differentially expressed genes (DEGs) encoding ion channels, neurotransmitter receptors, and calcium-binding proteins across molecularly distinct clusters, further underscoring the molecular diversity generated by distinct differentiation strategies (Figure 1E and Table S2). Notably, expression of the NMDAR subunits *GRIN2A* and *GRIN2B* was higher in neurons produced with the small-molecule patterning (Figure S3B). *GRIN2B* is predominantly expressed during prenatal cortical development, whereas *GRIN2A* expression emerges largely postnatally.[52] This pattern aligns with prior reports demonstrating that combining regional patterning with lineage-specific TF induction promotes NMDAR subunit expression[33], suggesting a synergistic effect on neuronal maturation.

To annotate the brain regional identities represented by the iGABAs, we applied a reference-mapping approach using scRNA-seq datasets from primary human fetal brain regions,[53,54] including neocortex, GE, striatum, thalamus, hypothalamus, midbrain, and claustrum (see Methods). iGABAs mapped across multiple forebrain regions, including the hypothalamus, thalamus, neocortex, and GE (Figure 1F). While all differentiation strategies produced neurons spanning multiple regional identities, GE- and neocortex-associated populations were enriched in patterned ASCL1/DLX2 conditions (7D-patterned-iGABAs), whereas PSC-iGABAs generated without small-molecule patterning preferentially aligned with hypothalamic and thalamic identities. These assignments were supported by regional marker expression, including *FOXA2* in hypothalamic clusters[50,55] and *NR2F2* in the GE-associated cluster (Figure S3C).

Next, to benchmark interneuron diversity across differentiation strategies, we performed comparative single-cell transcriptomic analyses including 7D-patterned-iGABAs, PSC-iGABAs, and GABAergic neurons generated using previously published small-molecule–based protocols reported by other groups[45,56]. All datasets were uniformly annotated using the Feng et al. (2025) human developmental brain atlas, which resolves interneuron subtypes derived from MGE, LGE, and CGE origins across cortical and subcortical regions.[49] Across methods, human PSC-derived GABAergic neurons mapped to MGE-, CGE-, and LGE-associated lineages (Figure S4). However, neurons generated using small-molecule patterning protocols were strongly skewed toward MGE-derived interneuron subtypes, with limited representation of CGE- and LGE-associated populations. In contrast, both PSC-iGABAs and patterned-iGABAs spanned multiple developmental origins, yet interneurons assigned to the same MGE, CGE, or LGE domains

occupied distinct subtype states depending on the differentiation strategy, indicating that protocol choice shapes fine-grained interneuron identity beyond broad lineage assignment.

Functional Maturation and Circuit Integration of Patterned GABAergic iNs

Given transcriptomic evidence that 3D-patterned GABAergic iNs retain immature features, we focused subsequent analyses on 7D-patterned GABAergic induced neurons (hereafter referred to as GABAergic patterned iNs or patterned-iGABAs). To assess functional maturation *in vitro*, we performed whole-cell patch clamp recordings and immunofluorescence analyses at day 35 of differentiation (Figure 2A). Voltage-clamp recordings revealed prominent inward sodium currents in response to depolarizing steps (Figure 2B), and current-clamp traces showed robust trains of action potentials with increasing current injection (Figure 2C). Patterned-iNs exhibited passive membrane properties consistent with neuronal maturity (Figure 2D). To assess functional inhibitory synapse formation, we recorded spontaneous inhibitory postsynaptic currents (sIPSCs). sIPSCs were recorded in the presence of CNQX and abolished by application of picrotoxin, confirming GABAergic synaptic transmission (Figures 2E and 2F). Immunostaining further confirmed interneuron subtype diversity, including SST^+, CR^+, and CB^+ populations, together with expression of the cortical identity marker FOXG1 and the CGE-associated marker PAX6 (Figure 2G). Together, these results indicate that patterned-iN cultures generate functionally mature GABAergic neurons with diverse molecular, regional, and subtype identities.

To determine whether patterned-iNs can survive, mature, and integrate into neural circuits *in vivo*, we transplanted EGFP-labeled immature patterned-iNs into the periventricular region of neonatal $Rag2^{-}/^{-}$ mice. At five months post-transplantation, immunohistological analysis revealed that the majority of human nuclear antigen (HNA)–positive cells remained near the injection site and differentiated into $NeuN^+$ neurons, indicating stable neuronal maturation *in vivo* (Figures 3A and S5). To assess functional integration into host circuits, we performed whole-cell patch-clamp recordings from GFP^+ human neurons in acute cortical slices. Across 12 recorded cells from three animals, depolarizing current injections elicited robust action potential firing, with a mean rheobase of 30 ± 14 pA and firing frequencies reaching 42 ± 8 Hz at higher current steps (Figures 3B-D, Table S3). Action potentials exhibited mature biophysical properties, and passive membrane properties were consistent with mature functional interneurons (Figures 3E–J). Importantly, the human neurons received spontaneous synaptic inputs, including both excitatory postsynaptic currents (EPSCs) and inhibitory postsynaptic currents (IPSCs) (Figures 3K and 3L, Table S3), demonstrating synaptic connectivity with host cortical circuits.

Finally, immunohistochemical analysis using a human-specific synaptophysin antibody revealed presynaptic puncta associated with GFP^+ human neurons, providing additional evidence of synaptic connectivity *in vivo* (Figure 3M). Transplanted cells also displayed complex neuronal morphologies with elaborated dendritic arbors. Together, these findings demonstrate that patterned-iNs not only acquire functional maturity in vitro but also survive long term, receive synaptic inputs, and integrate into host cortical circuits following transplantation.

Neuropsychiatric and Neurological Disease Gene Enrichment Across GABAergic iN Types.

Induced neurons offer significant potential for studying neuropsychiatric and neurological diseases *in vitro* and for linking genetic risk to cellular phenotypes, offering valuable insights for basic research and pharmaceutical development. To evaluate the disease relevance of different GABAergic iN populations, we performed gene set enrichment analysis using Disease Enrichment (DisGeNET)[57] on shared and condition-specific genes expressed in PSC- or patterned-iGABAs. Our analysis revealed that genes shared between PSC- and patterned-iGABAs were strongly enriched for risk genes associated with various brain disorders, including intellectual disability, neurodevelopmental disorders (NDDs), schizophrenia, epilepsy, and bipolar disorder (Figure S6A; Table S4; q-value ≤ 0.05). Notably, genes specific to patterned iNs also showed strong enrichment in psychiatric and neurological conditions, whereas genes specific to PSC-iNs were preferentially enriched for non-neural disease annotations (Figures S6B and S6C). Consistent with this observation, patterned-iN-specific genes also exhibited robust enrichment for ASD risk genes curated in the SFARI database[58] (odds ratio = 2.50; BH-corrected $p = 1.05 \times 10^{-13}$). These findings indicate that while both PSC- and patterned iNs are suitable for investigating disease-associated genotype-phenotype relationships, patterned iNs exhibit closer alignment with neural lineages, making them particularly advantageous for modeling neural-related diseases. To further extend this analysis, we incorporated comparative transcriptomic mapping using publicly available scRNA-seq datasets derived from postmortem brain tissue of individuals with AD and ASD.[59,60] This approach enabled us to assess whether the transcriptional identities of induced GABAergic neurons correspond to interneuron populations implicated in these disease contexts. These analyses revealed overlap between patterned-iNs and disease-associated interneuron signatures observed in AD and ASD datasets, supporting their relevance for modeling disease-linked inhibitory neuron phenotypes (Figure S6D).

Gene Regulatory Networks Underlying Diverse GABAergic-Induced Neurons.

Next, to explore the regulatory mechanisms underlying GABAergic neuron identities generated by different differentiation strategies, we applied single-cell regulatory network inference and clustering (SCENIC), which infers TF–centered regulons and their target gene networks from scRNA-seq data.[61] This analysis identified both shared and strategy-specific regulons across PSC-iGABAs and patterned-iGABAs, revealing distinct gene regulatory architectures associated with each differentiation approach (Figure S7). At a global level, regulons associated with PSC-iGABAs included well-recognized determinants of interneuron cell fate and migration, such as DLX2 and DLX5. Regulons linked to 7D-patterned-iGABAs, such as NR2F1 (COUP-TFI), NR2F2 (COUP-TFII), and PAX6, are recognized for their roles in the differentiation of specific interneuron subtypes, including those originating from the LGE and CGE [13,62,63].

Because relatively few GABAergic neurons were recovered following 3-day DOX induction, we focused subsequent analyses on PSC-iNs and 7D-patterned iNs to identify specifically activated regulons within each molecular cluster. Neurons from these conditions were subdivided into molecular clusters based on transcriptomic profiles, and regulons were ranked using the Regulon Specificity Score (RSS) to identify cluster-enriched regulatory programs (Figures 3A and 3B). Our analysis revealed that each neuronal cluster was associated with different sets of regulons. Specifically, within the GABAergic PSC-iNs, prominent regulons included FOXA1, FOXA2, and PBX1, TFs associated with hypothalamic regionalization, neurogenesis, and neuroendocrine function. FOXA1 and FOXA2 emerged as primary regulons in cluster 1, consistent with their established expression in the embryonic hypothalamus and its role in regulating adaptive responses to metabolic state, such as fasting.[50,55] PBX1 has similarly been implicated in hypothalamic molecular pathways involved in hormonal regulation.[64] We also showed the expression patterns of these top-ranked regulators in corresponding neuronal clusters (Figure 3A). In addition, consistent with our observations that subsets of PSC-iNs exhibit striatal-like features, several highly expressed TFs associated with both striatal and hypothalamic differentiation and function were identified, including ONECUTs, MEIS2, and ISL1.[48,65,66]

In contrast, we found that subclusters of GABAergic neurons generated with patterning factors were enriched in a distinct set of regulons associated with the processes of neural fate determination and migration, including *NR2F1/2, DLX6*, *RARB*, *POU2F2*, *TCF12,* and *PAX6* (Figure 3B). Notably, NR2F1, NR2F2, and PAX6 are expressed in GE and play key roles in the development of cortical and ventromedial forebrain inhibitory neurons. Compared with PSC-iNs, patterned-iNs exhibited more homogeneous regulatory programs across clusters, reflected by

broader sharing of key regulons and reduced cluster-specific segregation (Figure 3C). Together, these analyses demonstrate that differentiation strategy shapes GABAergic neuron identity not only at the level of transcriptomic subtype composition but also through distinct gene regulatory networks, highlighting how TF–based induction and extrinsic patterning cues engage overlapping yet non-identical regulatory programs to generate diverse inhibitory neuron states.

Distinct Lineage-Specific Gene Regulatory Networks Induced by ASCL1&DLX2 in PSCs and Patterned Progenitors.

Epigenetic regulation plays a pivotal role in determining and specifying cell lineages. To gain insights into the regulatory mechanisms that drive the fate specification of PSC-iNs and patterned-iNs, we performed SHARE-seq (Simultaneous High-throughput ATAC and RNA Expression with Sequencing)[67] on PSCs, patterned progenitors, and cells at the early stages following ASCL1 and DLX2 induction (Figure 5A). This approach enabled simultaneous profiling of chromatin accessibility and gene expression within individual cells, providing a comprehensive view of the regulatory landscape underlying neuronal differentiation. We obtained high-quality ATAC-seq and RNA-seq data from 23,434 cells. To reveal global similarities and distinctions among individual cells, we applied dimensionality reduction using Latent Semantic Indexing (LSI) to single-cell ATAC-seq data and PCA to scRNA-seq data, followed by visualization using UMAP embedding. Chromatin accessibility and transcriptional representations were well aligned, revealing coherent trajectories that reflect the progression of cell states over time and segregate according to cell type of origin (Figure 5B).

To investigate the mechanisms governing the specification of GABAergic neurons derived from PSCs and patterned progenitors, we first reconstructed the trajectory of neuron development by assigning pseudotime values to individual cells and tracing their progression along their respective differentiation pathways (Figure 5C). As expected, cells treated using small molecules exhibited expression of neural progenitor cell (NPC) marker genes (e.g., *SOX2*, *NES*, *SOX11*, *PAX6*) (Figure S8). Following TF induction, genes associated with interneuron development, such as *OTX2*, *PROX1*, *TCF12*, and *RELN*, were robustly induced in the patterned progenitors and, to a lesser extent, in iPSCs (Figures 5C and S8). This expression pattern quickly transitioned towards a GABAergic neuronal identity, marked by the induction of *GAD1*, *GAD2*, *DLX6*, and related markers. In parallel, neuronal differentiation genes (e.g., *DCX, TUBB3, RBFOX3*, etc.) and genes encoding neurotransmitter receptors (*GRIA1-4*, *GRINA*, *GRIN2A*, *GABRA2/B2*, etc.) were induced, consistent with the rapid gene expression changes characteristic of TF-mediated cell fate conversion. To complement these analyses and assess

lineage specificity, we examined canonical markers of excitatory neuronal and glial lineages in both PSC-iNs and patterned-iNs. Markers of cortical excitatory neurons (*TBR1*, *EMX1*, *SLC17A6/7*) were undetectable across iGABAs. Similarly, astrocytic (*GFAP*, *AQP4*, *S100B*, *ALDH1L1*) and oligodendrocytic (*OLIG1*, *OLIG2*, *MBP*, *MOG*) markers were absent or expressed at negligible levels (Figure S9). *MBP* showed modest induction in PSC-iNs but not in patterned-iNs, suggesting a slightly higher propensity for glial gene activation in PSC-derived cells. Together, these data confirm efficient and selective induction of inhibitory neuronal identity by ASCL1 and DLX2 in both contexts, while revealing subtle differences in lineage restriction between differentiation strategies.

Genes active at later pseudotime stages were enriched for gene ontology (GO) terms related to neural morphogenesis, migration, and development (Figure 5C). In contrast, distinctive GO enrichments were associated with genes active at early and intermediate stages of differentiation trajectories over pseudotime, suggesting that ASCL1 and DLX2 induce context-dependent molecular programs in PSCs and patterned progenitors. Specifically, GO terms uniquely enriched among genes active early in the PSC-iN trajectory included non-neuronal processes, whereas genes induced in patterned iNs were associated with signaling pathways involved in neurogenesis, including WNT and VEGF signaling pathways [68-70].

Further analysis of the chromatin landscapes before and after TF induction revealed significant state-dependent remodeling, with distinct clusters of open chromatin peaks emerging across different cell states and stages of differentiation (Figure 5D). GO analysis of genes linked to these open chromatin regions showed that regions accessible in PSCs and patterned NPC-like cells but rendered largely inaccessible after ASCL1 and DLX2 induction were primarily associated with non-neuronal processes (clusters 4, 5). Conversely, regions that were initially inaccessible in PSCs or patterned cells but became accessible after TF induction were strongly enriched for neurogenesis (cluster 2). We also noted that transiently accessible regions were linked to stem cell differentiation (clusters 1, 8), whereas regions that became robustly accessible exclusively along the PSC-iN trajectory were occasionally associated with “off-target” regulator programs (clusters 3, 7). Together, these chromatin dynamics mirror the transcriptional changes observed following TF induction and indicate a more stringent and lineage-directed neuronal differentiation program in patterned NPC-like cells, compared with a more heterogeneous regulatory program in PSCs at early stages. These findings highlight the nuanced interplay between epigenetic and transcriptional regulation in shaping cell fate decisions.

We next examined TF-driven regulatory mechanisms across pseudotime by correlating TF expression with motif activity scores derived from chromatin accessibility. This analysis identified 37 TF motifs differentially associated with the progression along the PSC-iN or patterned-iN differentiation trajectories (Figure 5E). Both differentiation pathways showed strong activity of ASCL1 and DLX motifs, reinforcing their central roles in cell-fate determination. Additionally, motifs corresponding to TFs with established roles in neural development and function, including TCF12[71], CTCF[72,73], SP3[74], SP9[75], and KLF7[76,77], were active in both differentiation trajectories. In contrast, numerous other TF motifs, particularly those integral to pluripotency maintenance and broader lineage plasticity, such as POU4F1 (OCT4), MGA[78], SNAI2[79], TCF3[80], and MEIS3[81] were more specifically involved in the PSC-iN differentiation pathway. Collectively, these findings underscore the intricate coordination of TF motifs early in neuronal differentiation, supporting our observation that ASCL1 and DLX2 engage a more tightly constrained TF network in patterned progenitors, fostering a more defined path toward GABAergic neuronal differentiation. In contrast, PSCs retain greater plasticity, enabling activation of a broader spectrum of TF-driven gene expression networks. This distinction suggests that although both PSCs and patterned progenitors are competent for neuronal differentiation, the pathways and regulatory networks involved are significantly divergent, reflecting the intrinsic differences in their biological potential and responsiveness to transcriptional cues.

Disease Modeling Potential of Patterned Induced GABAergic Neurons.

To evaluate whether GABAergic patterned-iNs can be leveraged to uncover disease-relevant phenotypes, we focused on ADNP syndrome, a rare neurodevelopmental disorder caused by mutations in the *activity-dependent neuroprotective protein (ADNP)* gene and frequently associated with ASD. [82-84] GABAergic interneurons are central to regulating excitation–inhibition balance and network synchrony, processes commonly disrupted in ASD and related NDDs, yet the effects of ADNP mutations on human inhibitory neurons have not been well characterized.

Among individuals with ADNP syndrome, a recurrent heterozygous nonsense mutation at p.Tyr719* has been frequently identified.[82-84] To model this variant, we used CRISPR-Cas9 to introduce the ADNP p.Tyr719* allele into two independent human iPSC lines (PGP1 and WTC11). In parallel, a hemagglutinin (HA) tag was inserted at the 3’ end of the endogenous *ADNP* locus or immediately following the p.Tyr719* truncation to enable detection of full-length and truncated ADNP proteins. As shown in Figure S10, an ADNP antibody recognizing a region between residues 1,050 and the C-terminus detected full-length ADNP in both unedited and HA-

tagged control cells but not the truncated p.Tyr719* protein, whereas the truncated protein was readily detected using an HA antibody. Consistent with heterozygosity, levels of full-length ADNP were reduced in heterozygous p.Tyr719* mutant lines relative to unedited controls.

Patterned-iNs were generated from heterozygous and homozygous *ADNP* p.Tyr719* iPSCs and their corresponding isogenic controls (six lines in total) and analyzed five weeks after differentiation in glial co-culture by scRNA-seq. Following quality control and filtering, the WTC11 homozygous cells were excluded from subsequent analyses due to insufficient cell recovery. Patterned iNs derived from different genetic backgrounds exhibited high reproducibility (Figure S11A). Transcriptomic profiling revealed a high degree of correlation between heterozygous and homozygous mutant cells (Figures 6A and 6B), prompting us to combine mutant cells from both PGP1 and WTC11 lines to increase statistical power. Pan-neuronal markers, including MAP2 and RBFOX3 (NeuN), were robustly expressed in both wild-type and mutant neurons (Figure S11B), confirming successful neuronal differentiation. Assessment of neurotransmitter identity showed that the majority of neurons were GABAergic, with 98.62% of wild-type and 97.28% of mutant MAP2-positive neurons classified as GABAergic.

To assess cellular heterogeneity, we applied the Leiden clustering algorithm to identify transcriptomically distinct populations. This analysis revealed clear segregation between mutant and wild-type neurons, supported by statistically significant differences in gene expression (Table S5). Specifically, clusters 0 and 1 were predominantly composed of p.Tyr719* mutant cells, whereas cluster 2 was enriched for wild-type neurons (Figure 6C). We next examined maturation states by assigning pseudotime values using Monocle3, which identified cluster 0 mutant neurons as the least mature population (Figure 6D). This interpretation was supported by enrichment of *NESTIN* (*NES*), a marker commonly associated with neural progenitors, within this cluster (Table S5). A continuous differentiation trajectory within the mutant population was also observed and independently validated using Slingshot (Figure S11C). Along this trajectory, mutant neurons progressively upregulated genes encoding GABA and glutamate receptor subunits (*GABRB2*, *GRIA2*, *GRID2*), synaptic signaling components (*SYN3*, *DLG2*, *NRXN3*), and neuronal differentiation markers (*ROBO1*, *NRP2*), all of which are critical for neuronal maturation and synaptic transmission (Figure S11D; Table S6).

To further define molecular alterations associated with the p.Tyr719* mutation, we examined DEGs between mature mutant and wild-type cells using a pseudobulk analysis framework. Mutant neurons exhibited both downregulated and upregulated transcriptional programs (Figure 6E and Table S7). Notably, genes involved in the generation of CGE-derived

cortical interneurons, including *NR2F2* and *PROX1*, as well as genes associated with LGE-derived interneurons in the olfactory bulb and basal nuclei, such as *FOXP2,* and *CALB1*,[13] were significantly downregulated in the mutant cells. PAX6[13,49], which contributes to both CGE and LGE interneuron development, was also reduced. Conversely, *RELN*, primarily produced by specific subsets of GABAergic interneurons in the neocortex and hippocampus, was upregulated.[85,86] GO analysis of DEGs highlighted enrichment for pathways related to synaptic organization and neuronal connectivity, including regulation of postsynaptic membrane potential, synapse organization, trans-synaptic signaling, and cell–cell adhesion, as well as processes involved in neuronal development and maturation, such as regulation of neuron projection development and nervous system development (Figure 6F and Table S8).

To capture coordinated transcriptional changes associated with the p.Tyr719* mutation, we performed Weighted Gene Co-expression Network Analysis (WGCNA) focusing on clusters 0, 1, and 2. To mitigate the sparsity inherent in single-cell data while preserving the heterogeneity often masked by traditional cell clustering, we first constructed metacells[87], representing aggregates of cells with similar gene expression profiles, in which within-metacells variation is primarily technical rather than biological (Figure S12A). Subsequently, we constructed gene co-expression modules separately for the three clusters, identifying 25 gene co-expression modules (Figure S12B and Table S9). Modules associated with mutant neurons were enriched for biological processes including translational initiation, neuronal development, membrane potential regulation, and chemical synaptic transmission (Figure S12C).

Finally, to determine whether these transcriptional alterations translated into functional deficits, we performed whole-cell patch-clamp recordings on patterned GABAergic interneurons derived from three independent ADNP p.Tyr719* mutant clones and matched controls. Mutant neurons exhibited significantly reduced spontaneous and miniature inhibitory postsynaptic current (sIPSC and mIPSC) frequencies, indicating impaired inhibitory synaptic transmission (Figures 6G-K and Table S10). These deficits were consistent across three independent differentiation batches, demonstrating robustness across genetic backgrounds and experimental replicates. Collectively, these results show that the ADNP p.Tyr719* mutation disrupts interneuron maturation, subtype-associated gene expression, and inhibitory synaptic function in human patterned GABAergic neurons, supporting the utility of patterned-iNs as a platform for identifying mutation-specific mechanisms in neurodevelopmental disease.

DISCUSSION

Differentiating human stem cells into regional- and neurotransmitter-specific subtypes of human interneuron populations offers a promising platform for studying pathophysiology and potential therapeutic approaches for various diseases. This study presents a rapid and reproducible method for generating GABAergic neurons by integrating our TF-mediated PSC differentiation[27] with developmental patterning achieved by inhibiting SMAD and WNT signaling[36,42]. This method, akin to the direct conversion of PSCs into GABAergic neurons driven by ASCL1 and DLX2, yields a homogeneous population of cells with inhibitory identity. We provide an extensive, mineable single-cell transcriptomic resource encompassing GABAergic neurons generated using TF-based induction, small-molecule-only patterning, and combinatorial patterning plus TF approaches. Systematic comparison across these differentiation strategies reveals that each method yields GABAergic neurons with overlapping yet distinct molecular identities, developmental trajectories, and subtype compositions. Importantly, this diversity is not a limitation but a strength for disease modeling, as different neurodevelopmental and neuropsychiatric disorders are associated with dysfunction in certain interneuron subtypes and developmental programs. By enabling direct cross-method benchmarking, this dataset facilitates informed selection of PSC-derived GABAergic neuron models best suited for interrogating particular genes, pathways, or disease contexts. Additionally, the study demonstrates that this combinatorial approach produces disease-relevant GABAergic neuron types and applies it to investigate the pathobiology of ADNP syndrome.

SMAD and WNT inhibitors can induce forebrain lineages from human PSCs, including excitatory and inhibitory neurons.[36,42] By activating SHH signaling, progenitor cells can be ventralized to differentiate toward human cortical interneuron lineages.[42,43,45,56] However, the maturation of these progenitor cells requires a protracted time, as evidenced by scRNA-seq data. When ASCL1 and DLX2 are induced in PSCs exposed to SMAD and WNT inhibitors, homogeneous GABAergic neurons can be derived without the need for SHH or its agonist. The neurons derived under this condition represent multiple brain regions and are biased toward the cortical lineage. In contrast, PSC-iGABAs without patterning molecules exhibit a more prominent hypothalamic identity. Furthermore, the PSC-iGABAs are enriched for TF regulons associated with hypothalamic and striatal neurogenesis and function. On the other hand, patterned-iGABAs are enriched for TF regulons linked to neural fate determination and migration. This difference highlights the distinct developmental trajectories and functional specializations of the two types of iGABAs. Importantly, when transplanted into the neonatal mouse brain, patterned iGABAs survive long term and differentiate into mature neurons but remain largely localized near the injection site, a limited migration pattern consistent with prior

reports of PSC-iGABAs[27] and likely reflecting direct, postmitotic conversion driven by ASCL1 and DLX2 rather than expansion of migratory neuroblast populations. Notably, recent work utilizing barcoding tools for lineage tracing suggested that individual human cortical progenitors can produce both excitatory and inhibitory neurons.[88] Cortically-derived inhibitory neurons share transcriptional similarities with CGE-derived interneurons but lack definitive marker genes. Given the expression of *SP8* and *NR2F2* in the patterned iNs, it is possible that some of these neurons represent cortically-derived inhibitory neurons.

The differential gene expression programs observed in PSC-iGABAs and patterned-iGABAs generated through ASCL1 and DLX2 overexpression highlight the complexity of transcriptional regulation in neurogenesis. Multiple factors may contribute to these differences. One of the primary reasons is the differences between the epigenetic landscapes of PSCs and NPC-like cells obtained by SMAD and WNT inhibition. PSCs possess a more open and plastic chromatin structure, allowing a broader range of TF binding sites to be accessible. In contrast, NPCs have a more restricted chromatin landscape, with specific regions pre-configured for neural differentiation. ASCL1, as a pioneering factor, can bind to closed chromatin regions and initiate chromatin remodeling. However, the function of pioneering factors is heavily influenced by cellular context. In PSCs, ASCL1 can access and activate a wide array of genes, leading to diverse gene expression profiles that may even include non-neuronal lineages. Conversely, the chromatin landscape in the NPCs is already more accessible in regions relevant to neural development, so ASCL1 and DLX2 primarily enhance the existing neural gene expression program. PSCs and NPCs also differ in their baseline transcriptional states. PSCs express genes associated with pluripotency and self-renewal, whereas NPCs are committed to a neural lineage and express genes characteristic of neural progenitor cells. When ASCL1 and DLX2 are introduced into these different contexts, the downstream targets they activate are influenced by the pre-existing transcriptional milieu. ASCL1 and DLX2 might interact with pluripotency factors and other non-neural transcriptional networks, leading to a more heterogeneous response in PSCs. Meanwhile, these TFs reinforce and enhance the neural differentiation program in NPCs, leading to a more focused and streamlined gene expression profile. This aligns with the observation that GABAergic patterned-iN subtypes are less molecularly distinguishable. Additionally, the availability of cofactors and interaction partners in PSCs and NPC-like cells can further modulate the activity of ASCL1 and DLX2, contributing to the observed differences in gene expression programs.

Finally, we leveraged patterned human GABAergic interneurons to investigate the phenotypic consequences of the ADNP syndrome-associated p.Tyr719* variant. ADNP is ubiquitously expressed and functions as a chromatin-associated regulator of gene expression through interactions with multiple partners, including CHD4, a core component of the nucleosome remodeling and deacetylase (NuRD) complex.[89,90] Together with CHD4 and HP1γ, ADNP forms the ChAHP complex, which represses transcription at specific genomic loci.[89] In *Adnp* knockout embryonic stem (ES) cells and mouse embryos, defects in neuronal fate specification have been observed,[89] and impaired excitatory and inhibitory synapses have been reported in juvenile *Adnp* haploinsufficient mice.[91] However, most existing *in vivo* studies rely on large exonic deletions that do not reflect the molecular nature of pathogenic human ADNP mutations. Large-scale genetic studies of ASD and developmental delay disorders have revealed a striking enrichment of *de novo* protein-truncating variants in *ADNP*, with a strong bias toward mutations located in the terminal exon, including the highly recurrent p.Tyr719* variant. These mutations are predicted to escape nonsense-mediated decay, and mutant *ADNP* transcripts have been detected in patient-derived samples, including peripheral blood, suggesting that truncated proteins are expressed. [84,92] Consistent with this prediction, we used endogenous HA tagging to directly demonstrate stable expression of the truncated ADNP protein from the native locus in human cells, providing direct evidence that pathogenic ADNP truncations are not simple loss-of-function alleles. This observation supports the possibility that disease-causing *ADNP* mutations may exert dominant-negative or gain-of-function effects, a mechanistic distinction that is not captured by deletion-based models.

Consistent with this interpretation, our data suggest that the p.Tyr719* variant not only alters the specification of neuronal subtypes within the GABAergic lineage but may also disrupt synaptic transmission in differentiated cells. Notably, we observed a high degree of transcriptional similarity between heterozygous and homozygous p.Tyr719* mutant interneurons, in contrast to prior reports showing minimal transcriptional differences between wild-type and heterozygous conditional Adnp knockout animals.[89] One plausible explanation is that, unlike the removal of exon 5, which encodes all but 67 of Adnp's 1108 total amino acids, the truncated ADNP protein produced by p.Tyr719* competes with full-length ADNP for chromatin binding sites or interacting partners, thereby perturbing gene regulatory networks in a manner distinct from simple dosage reduction.[89] Intriguingly, we observed upregulation of *CHD4* expression in mutant cells, a phenomenon not reported in *Adnp* knockout models (Figure S10B). Given that p.Tyr719* interacts with CHD4, this upregulation may reflect compensatory responses to the

sequestration of CHD4 by p.Tyr719*. Further studies will be required to define the precise molecular mechanisms underlying these effects.

Overall, our study expands the toolbox for disease modeling by demonstrating the complementary strengths of PSC-iNs and patterned iNs in representing different brain regions and disease contexts. This dual approach offers a robust platform for investigating the molecular mechanisms underlying a variety of neurodevelopmental and neuropsychiatric disorders.

Acknowledgments

This work was supported by NIH awards 5R21MH119580 (N.Y.), 5R01NS116057 (N.Y.), R21MH131600 (J.D.B., N.Y.), 5R01AA023797 (Z.P.P), and 5R01MH125528 (Z.P.P). This study was supported in part by a grant from the Simons Foundation (SFI-AN-AR-Pilot-00009949) (J.D.B.), Oxford-Harrington Rare Disease Scholar Award (J.D.B.), ADNP Foundation, and Seaver Foundation. X. W. is supported as a Seaver Foundation Fellow and by NARSAD Young Investigator grants (31904). R.H. is a Seaver Postdoctoral Fellow. L.L.B. was supported by the Training Program in Stem Cell Biology fellowship from the New York State Department of Health (NYSTEM-C32561GG). M.Y. is supported by a diversity supplement (3R01MH129372-03S1). M.L. is supported by the NIH F31 Ruth L. Kirschstein National Research Service Award (F31NS137751).

Author contributions

Conceptualization, R.H., L.L.B., J.D.B., S.M., and N.Y.; Methodology, R.H., L.L.B., and Y.T.; Investigation, R.H., Y.T., B.Z., J.L., X.L., R.D., M.L., G.I.G., and N.Y.; Formal Analysis and Data Visualization, L.L.B., M. Y., P.C., Y.S., J.L., X.L., X.W., A.T., and S.M.; Writing, R.H., L.L.B., J.L., X.L., X.W., S.M., and N.Y.; Supervision, X. W., A.T., J.D.B., P.J., Z.P.P., S.M., and N.Y.

Declaration of interests

The authors declare no competing interests.

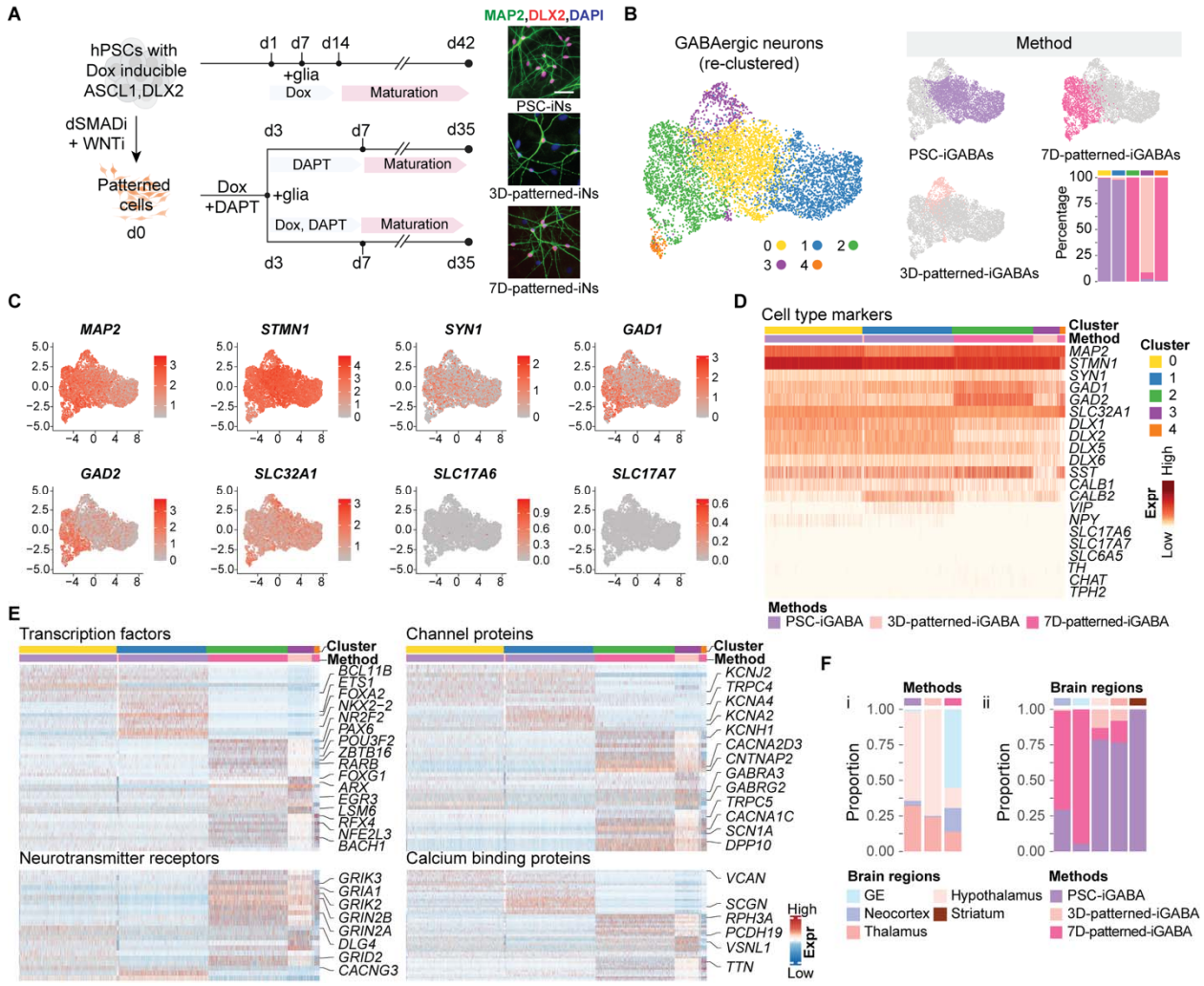

Figure 1. Generation of Diverse GABAergic iNs Using Different Strategies. (**A**) Schematic of the differentiation protocols used to generate GABAergic iNs from hPSCs using either TFs only (PSC-iGABA) or small molecule patterning followed by ASCL1/DLX2 induction (3D- and 7D-patterned-iGABAs). Representative immunofluorescence images show co-expression of MAP2 and DLX2 in all three conditions. Scale bar, 50 µm. Abbreviations: dSMADi (dual SMAD inhibition), WNTi (WNT inhibition), PSC-iNs (PSC-derived induced neurons), 3D-patterned-iNs (patterned induced neurons with 3 days of doxycycline exposure), and 7D-patterned-iNs (patterned induced neurons with 7 days of doxycycline exposure). (**B**) UMAP embedding of *SCL32A1*$^{+}$ GABAergic iNs, color-coded by cluster identity and differentiation method. Right: Cluster distribution for each method, with corresponding bar plot showing the percentage of cells from each condition in each cluster. (**C**) Feature plots showing inhibitory and excitatory neuron marker gene expression in GABAergic-induced neurons. (**D, E**) Heatmap of cell type-specific markers, TFs, channel proteins, neurotransmitter receptors, and calcium-binding protein

expression within each GABAergic iN cluster. The selected genes are implicated in psychiatric and neurological conditions, with a particular focus on ASD and epilepsy. (**F**) i. Proportions of cells from each method mapped to different brain regions using label transfer from primary human fetal brain datasets. ii. Contribution of each method to cells annotated as each brain region. Aggregated proportions showing that GE- and cortex-like cells are most enriched in 7D-patterned-iNs, whereas PSC-iGABAs show higher mapping to the hypothalamus and thalamus. See also Figures S1, S2, S3, Table S2.

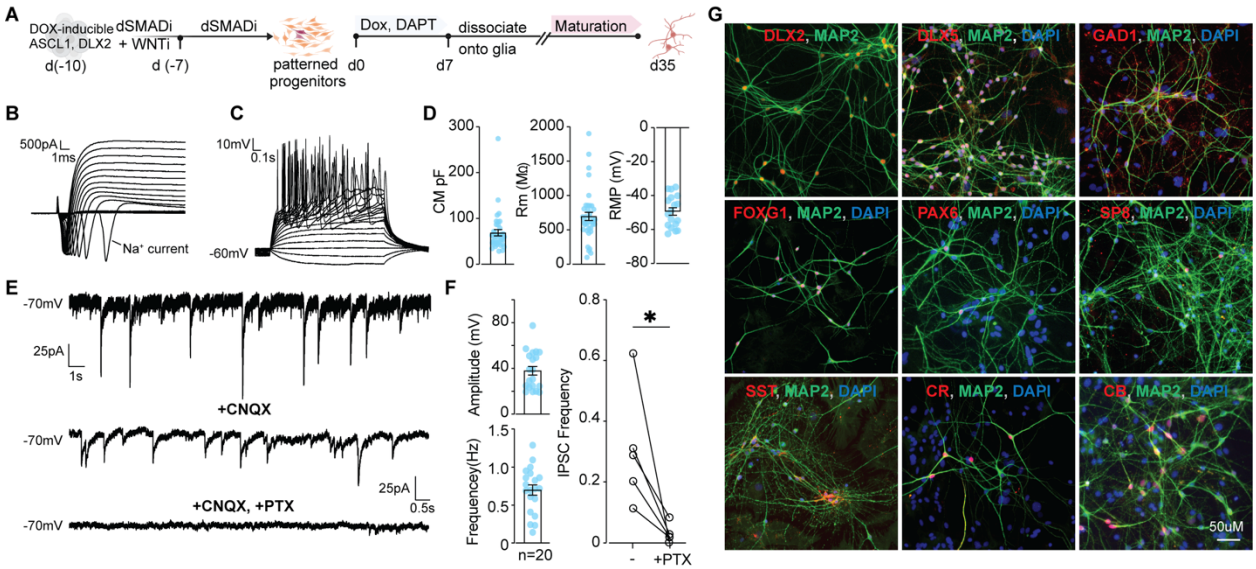

Figure 2. Functional and Subtype Characterization of patterned-iGABA Neurons. (**A**) Schematic of the differentiation protocol. (**B**) Voltage-clamp recording of inward sodium currents evoked by step depolarizations. (**C**) Current-clamp recording showing repetitive action potential firing across injected current steps. (**D**) Summary of passive membrane properties: membrane capacitance (CM) (n = 38), input resistance (Rm) (n = 38), and resting membrane potential (RMP) (n = 20). Each dot represents an individual recorded neuron. (**E**) Voltage-clamp recordings of spontaneous inhibitory postsynaptic currents (sIPSCs) at −70 mV. CNQX partially blocks EPSCs, and complete blockade is achieved with CNQX + picrotoxin (PTX). (**F**) Quantification of sIPSC amplitude and frequency across individual neurons (n = 20), with a significant decrease in IPSC frequency following PTX treatment ($p < 0.05$). (**G**) Immunofluorescence staining confirms the presence of multiple interneuron subtypes, including GAD1+, PAX6+, FOXG1+, SST+, CR+, and CB+ cells, co-labeled with MAP2. Scale bar: 50 µm.

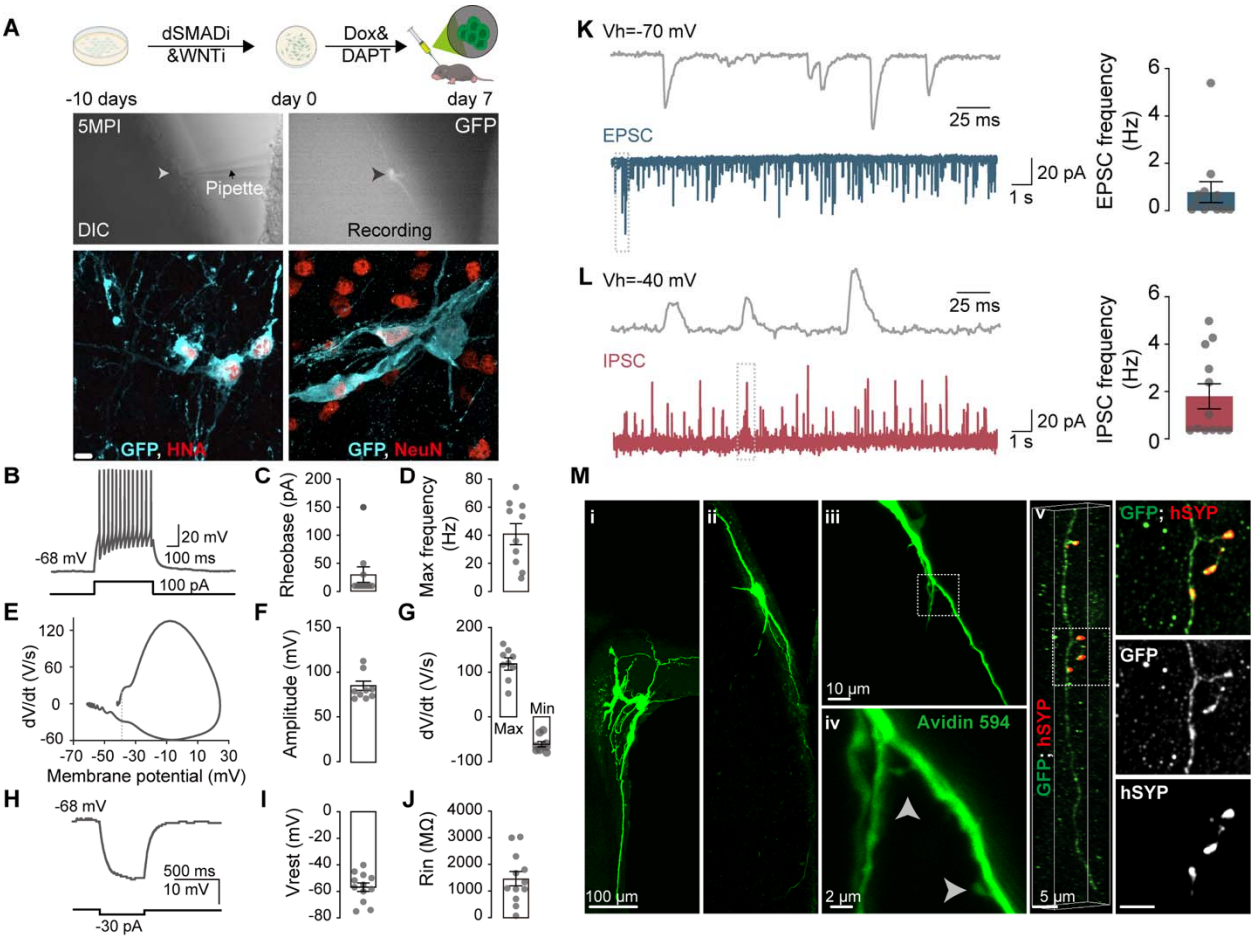

Figure 3. Functional and morphological characterization of human iPSC-derived interneurons following transplantation into the mouse cortex. (**A**) Top: Schematic overview and experimental timeline. Human iPSCs were patterned with dual SMAD and WNT inhibition (dSMADi & WNTi) for 10 days, followed by doxycycline (Dox) and DAPT treatment for 7 days, and subsequently transplanted into the cortex of postnatal day 2 (P2) immunodeficient mice. Whole-cell patch-clamp recordings were performed approximately 5 months post-injection (MPI). Middle left: Differential interference contrast (DIC) image of an acute brain slice showing a patch pipette approaching a GFP+ human induced neuron (iN). Arrowhead indicates the soma targeted for recording. Middle right: Fluorescent image of the same GFP+ neuron during patch-clamp recording. Bottom: Confocal images showing the GFP+ neurons (cyan) co-labeled with human nuclear antigen (HNA) or NeuN (red), confirming human neuronal identity. Scale bar: 5 µm. (**B**) Representative current-clamp recording from a GFP+ human neuron showing APs in response to a 500 ms, 100 pA current injection. Scale: 20 mV, 100 ms. (**C**) Group data showing rheobase values from 10 neurons (3 mice). (**D**) Maximum firing frequency of APs across the same group of GFP+ neurons. (**E**) Example phase-plane plot (dV/dt vs. membrane potential) of

a single AP from a GFP+ cell. (**F**) Group analysis of AP amplitude (left) and the maximal and minimal dV/dt slopes (right). (**G**) Voltage response of a GFP+ neuron to a 500 ms, -30 pA hyperpolarizing current step. Scale: 10 mV, 500 ms. (**H**) Group data showing resting membrane potential (V_rest) and input resistance (R_in) of GFP+ neurons (n=12 cells from 3 mice). (**K, L**) Representative voltage-clamp recordings showing spontaneous excitatory (**K**) and inhibitory (**L**) postsynaptic currents in GFP+ human neurons. Excitatory postsynaptic currents (EPSCs, blue) were recorded at a holding potential of –70 mV, while inhibitory postsynaptic currents (IPSCs, red) were recorded at a holding potential of –40 mV. Insets display expanded views of boxed regions to highlight individual synaptic events. Scale bars: 20 pA, 1 s (main traces), 25 ms (insets). Right panels: Quantification of spontaneous EPSC and IPSC frequencies in GFP+ neurons (n = 12 cells each). (**M**) Morphological reconstruction and synaptic marker localization in transplanted human interneurons. (**i–iv**) Biocytin–Avidin 594 staining of whole-cell recorded human GFP+ neurons reveals detailed cellular morphology. (i-ii) Overview of multiple recorded human neurons in the transplant region, filled with biocytin and visualized with Avidin 594 (green). (iii) High-magnification image of a single biocytin-filled neuron, showing its soma and dendritic arbor. (iv) Further magnified view highlights fine dendritic structures and spine-like protrusions (arrowheads). (v) Confocal z-projection showing co-localization of human-specific synaptophysin (hSYP, red), a presynaptic marker, along dendrites of a GFP+ interneuron (green). Split channels are shown below to confirm punctate hSYP localization on GFP-labeled neuronal processes. Scale bars: 100 µm (**i**), 10 µm (**ii–iii**), 2 µm (**iv**), 5 µm (**v**). Data are represented as mean ± SEM. See also Figure S5 and Table S3.

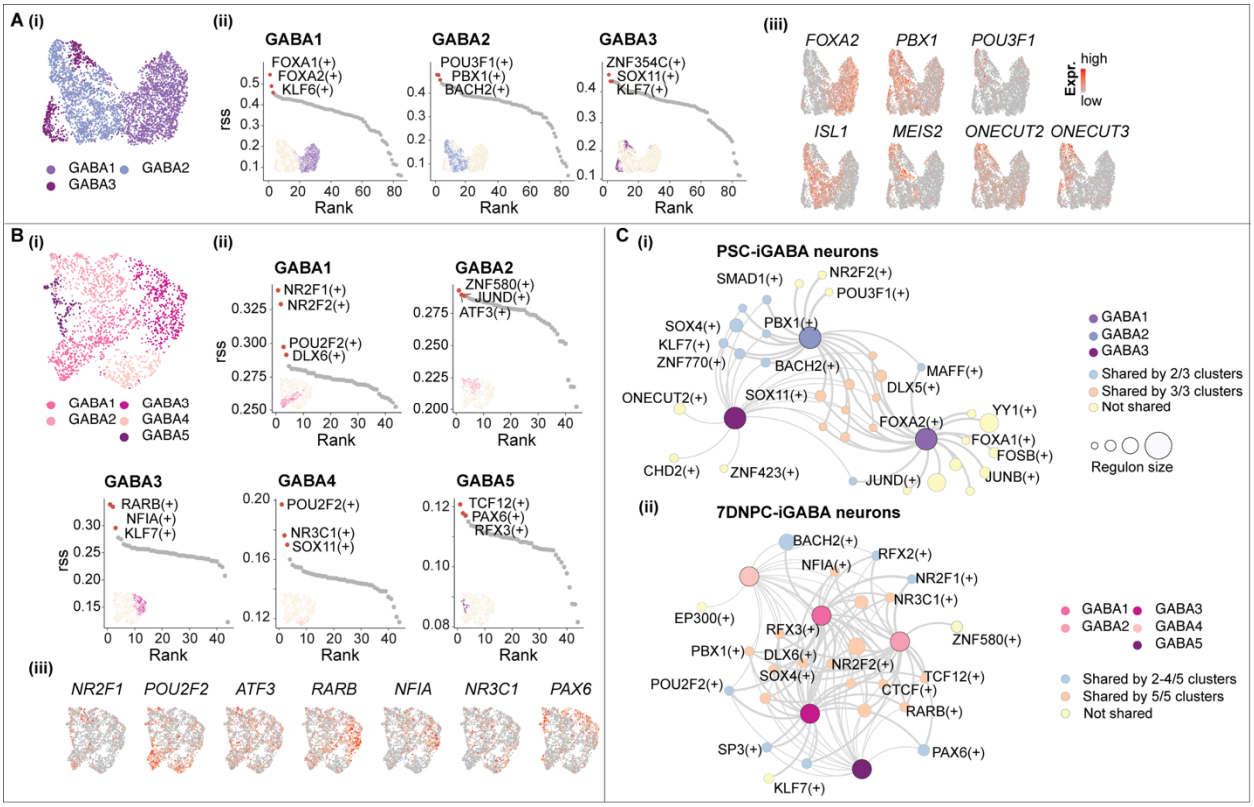

Figure 4. Gene Regulatory Networks Underlying Induced GABAergic Neuron Diversity. (A-B) Presented are the following for the GABAergic PSC-iNs (A) and the patterned iNs (B): (i) identified clusters, (ii) ranked regulons, and (iii) UMAP visualization of the top TFs associated with GABAergic neuron fate specification. **(C)** GRN analysis focused on cluster-specific modulators for **(i)** GABAergic PSC-iNs and **(ii)** patterned iNs. Regulons are color-coded by uniqueness, with node size proportional to the number of target genes regulated by each TF. Edge thickness indicates the strength of the association between a cluster modulator and its corresponding regulon. See also Figure S7.

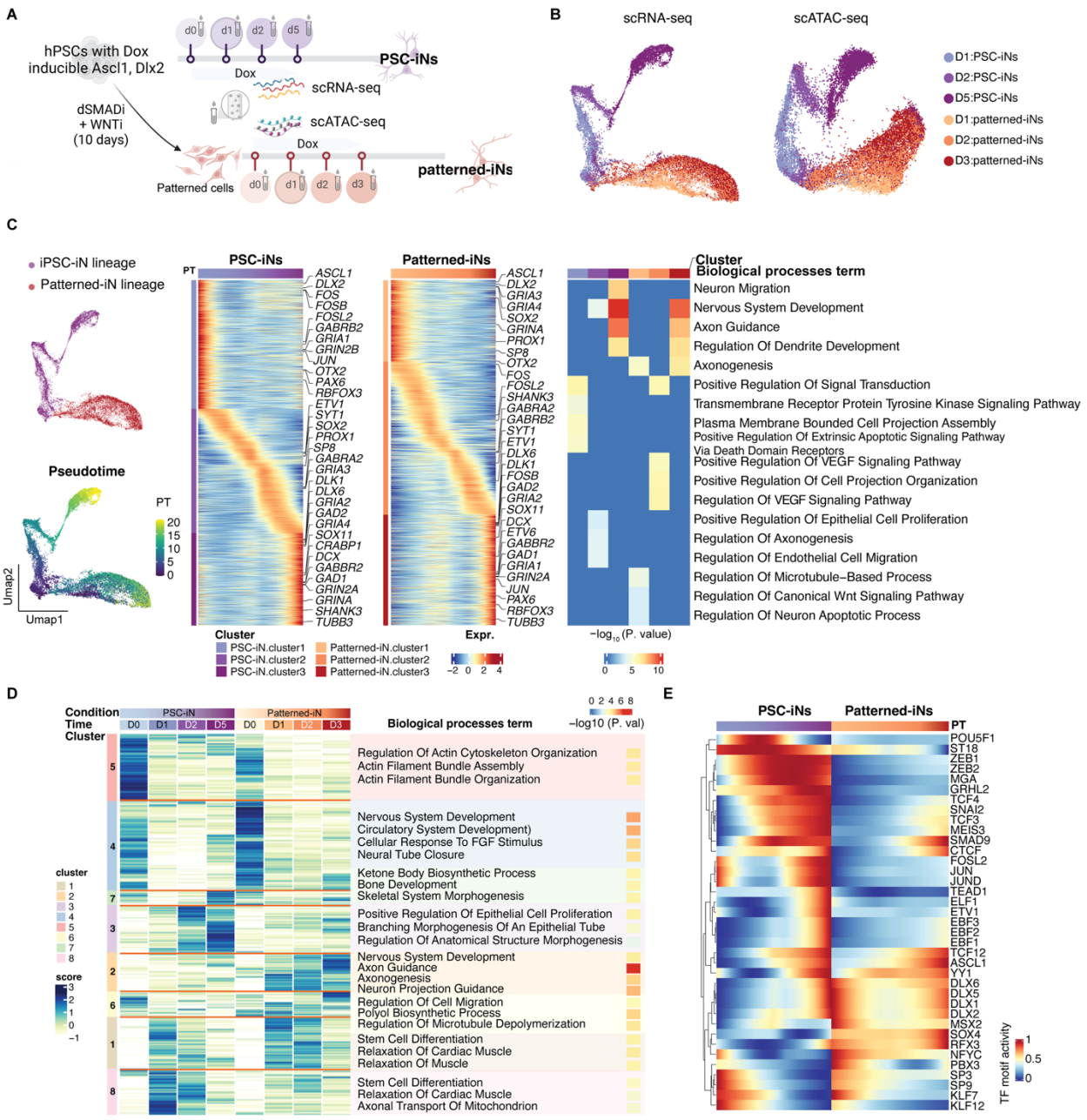

Figure 5. Molecular Signatures Underlying iN Specification. (A) Overview of the experimental workflow. **(B)** UMAP representations based on gene expression (left) and chromatin accessibility (right). Cells are color-coded according to differentiation time points and methods used. **(C)** UMAP of single-cell RNA sequencing (scRNA-seq) data highlighting the differentiation trajectory of PSC-iNs and patterned iNs, along with Slingshot-derived pseudotime (left). The middle panel shows a heatmap of gene expression across pseudotime bins within the PSC-iNs and patterned iNs trajectory. The right panel presents the Gene Ontology (GO) analysis of genes induced at various stages during early differentiation. **(D)** Heatmap showing

the chromatin accessibility across pseudobulk samples, aggregated from individual differentiation stages along the PSC-iNs and patterned iNs trajectory. The right panel shows the GO analysis of genes associated with accessible chromatin regions across the eight clusters. **(E)** Heatmaps showing motif activity of TFs across pseudotime bins. See also Figures S8 and S9.

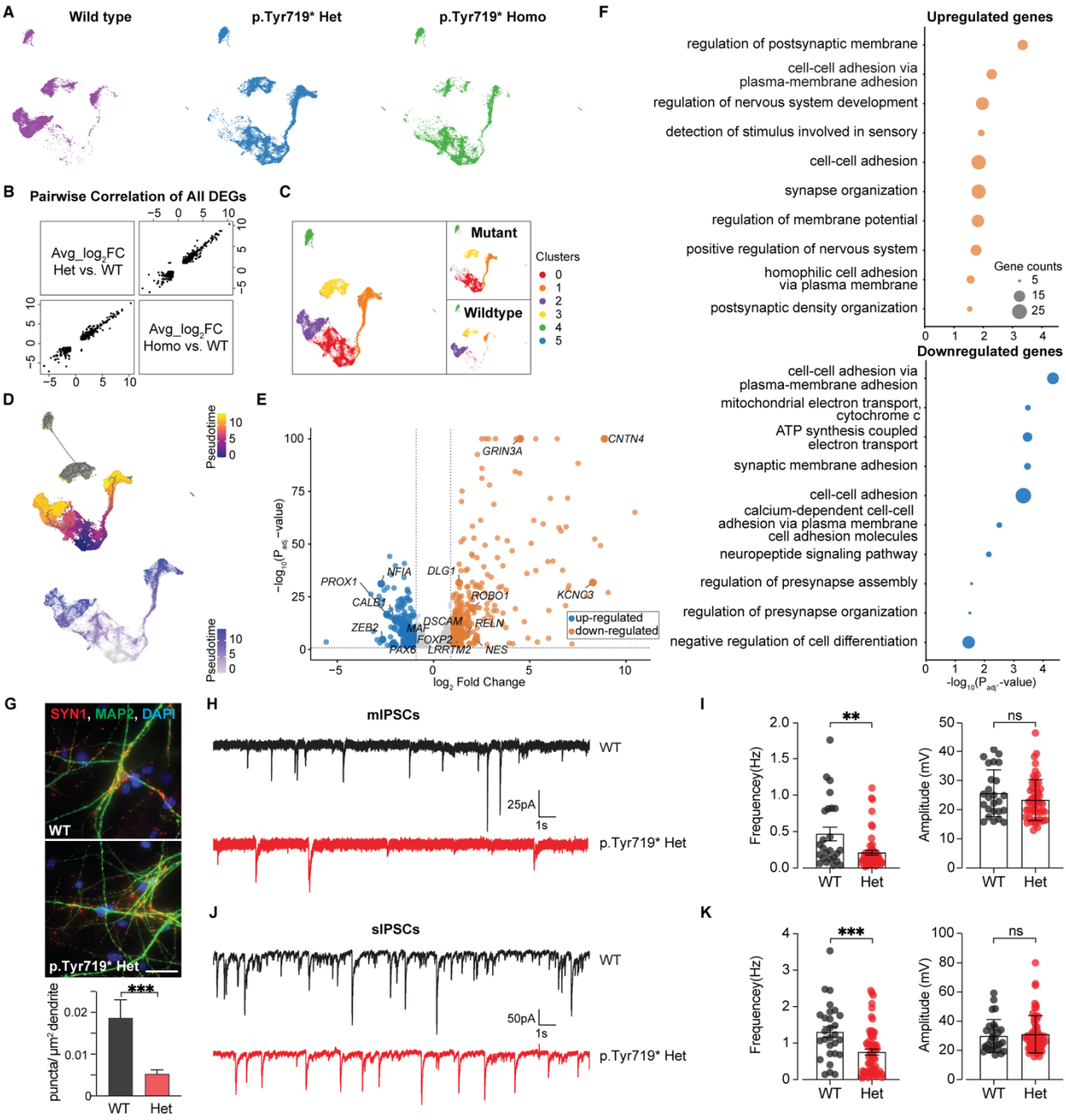

Figure 6. ADNP p.Tyr719 Mutation Disrupts Neurogenic and Synaptic Gene Expression and Function. (**A**) UMAP embedding of cells grouped by ADNP genotype (wild-type, heterozygous, and homozygous) across different iPSC lines, showing clustering by transcriptional similarity. (**B**) Pairwise correlation heatmap of all differentially expressed genes (DEGs) between wild-type and ADNPp.Tyr719* samples, indicating similar transcriptional changes caused by both heterozygous and homozygous ADNPp.Tyr719* mutations. (**C**) Combined UMAP of all single-cell transcriptomes reveals genotype-enriched clusters. Right: Same UMAP split by genotype, highlighting differences in cell distribution between WT and

ADNP-mutant cells. (**D**) Pseudotime UMAP analysis of all cell types (top), and pseudotime value of clusters 0, 1, and 2 identified in (C) (bottom). (**E**) Volcano plot displaying DEGs between ADNPp.Tyr719* and WT neurons (adjusted $p < 0.05$; $|\log_2 FC| > 1$). Selected upregulated and downregulated genes are annotated. (**F**) Top Gene Ontology (GO) Biological Process terms enriched among DEGs shown in (E), highlighting disruption of neurodevelopmental and synaptic programs. (**G**) Immunofluorescence images of SYN1 (synapsin 1), MAP2, and DAPI staining in WT and ADNP Het neurons. Right: Quantification of SYN1 puncta density per μm^2 of dendrite, revealing reduced synaptic density in ADNP Het neurons. Scale bar: 50 µm. (**H**) Representative traces of miniature inhibitory postsynaptic currents (mIPSCs) recorded from WT (blue) and ADNPp.Tyr719* heterozygous (Het, red) neurons. (**I**) Quantification of mIPSC frequency and amplitude from recordings in (**H**), across WT (blue, n = 25) and ADNP Het neurons (n = 61 from three batches). (**J**) Representative traces of spontaneous inhibitory postsynaptic currents (sIPSCs) recorded from WT and ADNP Het neurons. (**K**) Summary of sIPSC frequency and amplitude across pooled WT (n = 28 from three batches) and ADNP Het neurons (n = 61 from three batches), demonstrating significantly reduced inhibitory synaptic input in ADNP mutant cells. Data are shown as mean ± SEM. Statistical comparisons were made using one-way ANOVA (for multi-group) or unpaired t-tests (for two-group). *$P < 0.05$; **$P < 0.01$; ***$P < 0.001$. See also Figures S10, S11, S12 and Tables S5, S6, S7, S8, S9 and S10.

STAR Methods

Detailed methods are provided in the online version of this paper and include the following:

- **KEY RESOURCES TABLE**
- **RESOURCE AVAILABILITY**
  - Lead contact
  - Materials availability
  - Data and code availability
- **EXPERIMENTAL MODEL AND SUBJECT DETAILS**
  - Animal Model
  - Human PSC lines and culture
  - Lentivirus production
  - Small molecule-mediated GABAergic neuron generation
  - TF-mediated induced GABAergic neuron generation
  - Patterned induced GABAergic neuron generation
  - Lentivirus production
  - Lentivirus transduction
- **METHOD DETAILS**
  - Primary mouse astrocytes
  - Transplantation and brain slice preparation
  - Electrophysiological recordings from brain slices
  - Whole-cell recordings from cultured neurons
  - Immunofluorescence and imaging
  - Immunoblotting
  - 10X single-cell RNA-seq library preparation and sequencing
  - SHARE-seq library preparation and sequencing
- **QUANTIFICATION AND STATISTICAL ANALYSIS**
  - 10X Single-cell RNA-sequencing data processing and analysis
  - SHARE-seq data processing and analysis
  - Inferring regulatory networks
  - Gene Ontology, pathway enrichment, and disease-vulnerable cell type

- WGCNA analysis
- Statistical analyses

STAR ⍰ Methods

KEY RESOURCES TABLE

REAGENT or RESOURCE	SOURCE	IDENTIFIER
Antibodies		
Anti-ADNP	Bethyl Laboratories, Inc	Cat # A300-104A; RRID:AB_242522
Anti-HA	Roche	Cat #11867423001;RRID: AB_390918
Anti-CTCF	Cell Signaling Technology	Cat # 3418S; RRID:AB_2086791
Anti-HP1γ	Cell Signaling Technology	Cat # 2619S; RRID:AB_2070984
Anti-CHD4	Bethyl Laboratories, Inc	Cat # A301-081A; RRID:AB_873001
Anti-MAP2	Abcam	Cat # ab5392; RRID:AB_2138153
Anti-Synapsin	Synaptic Systems	Cat # 106 002; RRID:AB_887804
Anti-FOXG1	Takara Bio	Cat # M227; RRID:AB_2827749
Anti-Sox2	R&D Systems, Inc.	Cat # AF2018; RRID:AB_355110
Anti-Pax6	BioLegend	Cat # 901301; RRID:AB_2565003
Anti-H3K27ac	Abcam	Cat # AB4729; RRID:AB_2118291
Anti-IgG	Abcam	Cat # AB46540; RRID:AB_2614925
Anti-IgG	Novus Biologicals, LLC	Cat # NBP1-2763
Anti-FOS	Abcam	Cat # AB208942; RRID:AB_2747772
Anti-GAPDH	Cell Signaling Technology	Cat # 2118; RRID:AB_561053
Anti-β-actin	Sigma-Aldrich	Cat # A5441p RRID:AB_476744
Anti-Dlx5	(Wang et al., 2010)	Gift from John LR Rubenstein.
Anti-Dlx2	Santa Cruz Biotechnology, Inc	Cat # sc-393879
Anti-GAD67	Millipore	Cat# MAB5406, RRID:AB_2278725
Anti-CALB2	Agilent	Cat# M7245, RRID:AB_2068519
Anti-Calbindin	Swant	Cat# 300, RRID:AB_10000347
Anti-Pax6	Covance	Cat# PRB-278P, RRID:AB_291612
Anti-Somatostatin	Novus	Cat# NBP2-37447, RRID:AB_2890053
Anti-Human Nuclear Antigen	Milipore	Cat# MAB1281, RRID:AB_94090
Anti-SP8	Santa Cruz Biotechnology	Cat# sc-104661, RRID:AB_2194626
Anti-Synaptophysin	Thermo Fisher Scientific	Catalog # 14-6525-82; RRID:AB_10670280
Anti-NeuN	Millipore	Cat# MAB377, RRID:AB_2298772
Peroxidase-AffiniPure Donkey Anti-Rabbit IgG	Jackson ImmunoResearch Labs	Cat# 711-035-152, RRID:AB_10015282

IRDye 680RD Donkey anti-Mouse IgG	LI-COR Biosciences	Cat# 926-68072, RRID:AB_10953628
IRDye 800CW Goat anti-Rat IgG	LI-COR Biosciences	Cat# 926-32219, RRID:AB_1850025
Donkey anti-Mouse IgG 488	Thermo Fisher Scientific	Cat# A-21202, RRID:AB_141607
Donkey anti-Mouse IgG 555	Thermo Fisher Scientific	Cat# A-31570, RRID:AB_2536180
Donkey anti-Rabbit IgG 555	Thermo Fisher Scientific	Cat# A-31572, RRID:AB_162543
Donkey anti-Rabbit IgG 488	Thermo Fisher Scientific	Cat# A-21206, RRID:AB_2535792
Donkey anti-Chicken IgG 647	Thermo Fisher Scientific	Cat# A78952, RRID:AB_2921074
Chemicals, peptides, and recombinant proteins		
Stemflex supplement	Gibco | Thermo Fisher Scientific	Cat # A33492
Stemflex basal media	Gibco | Thermo Fisher Scientific	Cat # A33493-01
MEM media	Gibco | Thermo Fisher Scientific	Cat # 11090-081
Neurobasal media	Gibco | Thermo Fisher Scientific	Cat # 21103-049
Naurobasal A media	Gibco | Thermo Fisher Scientific	Cat # 10888-022
DMEM/F12 media	Gibco | Thermo Fisher Scientific	Cat # 11320-033
DMEM media	Gibco | Thermo Fisher Scientific	Cat # 11965-092
Knockout DMEM	Gibco | Thermo Fisher Scientific	Cat # 10829018
B27 supplement	Gibco | Thermo Fisher Scientific	Cat # 17504-044
N2 supplement	Gibco | Thermo Fisher Scientific	Cat # 17502-048
KnockOut™ Serum Replacement	Gibco | Thermo Fisher Scientific	Cat # 10828028
MEM NEAA (100x)	Gibco | Thermo Fisher Scientific	Cat # 11140-050
Glutamax (100x)	Gibco | Thermo Fisher Scientific	Cat # 35050-061
Sodium Pyruvate (100x)	Gibco | Thermo Fisher Scientific	Cat # 11360-070
β-Mercaptoethanol	Sigma-Aldrich	Cat # M3148
Cosmic Calf™ Serum	Cytiva	Cat # SH3008704
Fetal Bovine Serum	Sigma-Aldrich	Cat # F6178
D-PBS tablets	Millipore	Cat # 524650-1EA
Geltrex	Gibco | Thermo Fisher Scientific	Cat # A14133-02
Poly-L-ornithine hydrobromide	Sigma-Aldrich	Cat # P3655
Accutase	Innovative Cell Technologies	Cat # AT104500
Trypsin 0.25%	Gibco | Thermo Fisher Scientific	Cat # 25200-114
Puromycin dihydrochloride	Sigma-Aldrich	Cat # P8833
Hygromycin B (50 mg/mL)	Gibco | Thermo Fisher Scientific	Cat # 10687010
Cytosine β-D-arabinofuranoside	Sigma-Aldrich	Cat # C1768

Doxycycline	Sigma-Aldrich	Cat # P3655
Bovine Serum Albumin	Equitech-Bio Inc	Cat # BAH65-0500
Thiazovivin	Santa Cruz Biotechnology, Inc	Cat # SC-361380
Y-27632	Tocris Bioscience	Cat # 1254
Chroman1	MedChemExpress LLC	Cat # HY-15392
LDN193189	Stemgent	Cat # 04-0074
SB431542	Tocris Bioscience	Cat # 1614
XAV939	Stemgent	Cat # 04-0046
DAPT	Tocris Bioscience	Cat # 2634
SHH	R&D Systems	Cat # 1845-SH
Purmorphamine	R&D Systems	Cat # SML0868
Dimethyl sulfoxide	Sigma-Aldrich	Cat # D2438
Paraformaldehyde solution	Affymetrix	Cat # 19943
Halt Protease and Phosphatase Inhibitor Cocktail	Thermo Fisher Scientific	Cat # 78440
Critical commercial assays		
Pierce RIPA Buffer	Thermo Fisher Scientific	Cat # 89900
Bolt™ 4 to 12%, Bis-Tris, Protein Gel	Thermo Fisher Scientific	Cat # MW04125BOX
iBlot™ 2 Transfer Stacks, PVDF	Thermo Fisher Scientific	Cat # IB24001
Western Lightning Plus, Chemiluminescent Substrate	Revvity Health Sciences Inc	Cat # NEL104001EA
Pierce™ BCA Protein Assay Kits	Thermo Fisher Scientific	Cat # 23225
Intercept® (PBS) Blocking Buffer	LI-COR bio	Cat # P/N: 927-70001
Bio Rad ChemiDoc MP Imaging System	Bio Rad	RRID:SCR_019037
Chromium Next GEM Single Cell 3’ GEM Kit v3.1	10X Genomics	Cat # PN-1000123
Chromium Next GEM Single Cell 3’ Gel Bead Kit v3.1	10X Genomics	Cat # PN-1000122
Chromium Next GEM Chip G Single Cell Kit	10X Genomics	Cat # PN-1000120
Chromium iX	10X Genomics	Cat # PN-1000328, RRID:SCR_024536

ZEISS LSM 980 with Airyscan 2 Microscope	ZEISS	RRID:SCR_025048
EVOS M5000 Imaging System	ThermoFisher Scientific	Cat # AMF5000, RRID:SCR_023650
Deposited Data		
Raw single cell-sequencing data and normalized counts	This paper	GSE277602 and GSE277604
Experimental models: cell lines		
PGP1	Coriell	Cat# GM23338, RRID:CVCL_F182
WTC11	Coriell	Cat# GM25256, RRID:CVCL_Y803
HES-3 NKX2.1GFP/w	Goulburn A.L., et al., 2011[93]	RRID:CVCL_A5HB
HEK293T	ATCC	Cat # 11268, RRID:CVCL_1926
Experimental models: organisms/strains		
CD1 mouse strain	Charles River	Cat# CRL:022, RRID:IMSR_CRL:022
Recombinant DNA		
FUW-M2rtTA	Hockemeyer et al., 2008[94]	RRID:Addgene_20342
TetO-Ascl1-puro	Yang et al., 2017[27]	RRID:Addgene_97329
TeoO-Dlx2-Hygro	Yang et al., 2017[27]	RRID:Addgene_97330
pMD2.G	Addgene	RRID:Addgene_12259
pRSV-rev	Addgene	RRID:Addgene_12253
pMDLg/pRRE	Addgene	RRID:Addgene_12251
PB-TO-ASCL1-DLX2	Addgene	RRID:Addgene_182307
Software and algorithms		
Cellranger v7.2.0	10x Genomics	RRID:SCR_023221
ClusterProfiler v4.8.3	Yu et al., 2012[95]	RRID:SCR_016884
DoubletFinder v2.0.4	McGinnis et al., 2019[96]	RRID:SCR_018771
Gephi v0.10.1	http://gephi.org/	RRID:SCR_004293
ggplot2 v3.4.3	Wickham, 2016[97]	RRID:SCR_014601
Metacell	Baran et a., 2019[87]	RRID:SCR_017013
Monocle3	Cao et al., 2019[98]	RRID:SCR_018685
ZEISS ZEN Microscopy Software	ZEISS	RRID:SCR_013672
R	Love et al., 2014[99]	https://www.r-project.org/
Revigo v1.8.1	Supek et al., 2011[100]	RRID:SCR_005825
RStudio v4.3.1	Rstudio team, 2020[101]	https://github.com/rstudio/
Seurat v4.0.1.	Butler et al., 2018[102]	RRID:SCR_016341

SingleCellExperiment v1.22.0	Amezquita et al., 2020[103]	https://github.com/drisso/SingleCellExperiment
Slingshot v2.8.0	Street et al., 2018[104]	RRID:SCR_017012

RESOURCE AVAILABILITY

Lead contact

Further information and requests for resources and reagents should be directed to and will be fulfilled by the Lead Contact, Nan Yang (nan.yang1@mssm.edu).

Materials availability

The plasmids and cell lines generated in this study will be made available on request upon the completion of a Material Transfer Agreement (MTA).

Data and code availability

Single-cell RNA-seq and SHARE-seq data have been deposited at GEO and are publicly available as of the date of publication. Accession numbers are listed in the key resources table. The DOI is listed in the key resources table. This paper does not report original codes. Any additional information required to reanalyze the data reported in this paper is available from the lead contact upon request.

EXPERIMENTAL MODEL AND SUBJECT DETAILS

Animal Model

All animal experiments were approved by the Institutional Animal Care and Use Committee and were conducted in compliance with the relevant ethical regulations. Mice were maintained in social cages on a 12-hour light/dark cycle with free access to food and water; animals were monitored daily for food and water intake. Wild-type CD1 mice were used to isolate primary cell cultures on postnatal day 3 (P03). Animals of both sexes were used in the analyses.

Human PSC lines and cell culture

Human PSCs were maintained on Geltrex-coated plates in Stemflex medium and a 5% CO2 environment at 37ºC. Cells were passaged using Accutase in Stemflex supplemented with Chroman1 (2 μM), which was removed from the media the following day.

To generate genetically modified PGP1 and WTC11 iPSCs with the *ADNP* p.Tyr719* variant, we altered the nucleotide sequence NM_015339.4.2157C to G. Additionally, we inserted hemagglutinin (HA) tags immediately after Tyr719 to detect the resulting truncated proteins. In parallel, as a control, we inserted HA tags at the 3’ end of the endogenous ADNP gene in the PGP1 line. sgRNAs targeting proximal regions were designed using the CHOPCHOP online tool

(https://chopchop.cbu.uib.no/) and cloned into the lentiCRISPRv1 plasmid (Addgene Plasmid #49535) using the Golden Gate Assembly protocol. The gene-targeting template plasmid used to generate the HA-tagged *ADNP* p.Tyr719* allele includes a puromycin-resistance cassette flanked by LoxP sites for Cre-recombinase mediated deletion, positioned after the HA tag sequence, and the 5′ and 3′ DNA homology arms. A similar gene-targeting template was used to generate the HA-tagged *ADNP* allele. The day before transfection, human iPSCs were dissociated into single cells with Accutase and plated at 250,000 cells per well in six-well plates containing StemFlex medium with Chroman1. For transfection, the template vector (1 µg) and the CRISPRv1-gRNA (0.5 µg) were incubated with Lipofectamine Stem Transfection Reagent (10 µl) and OptiMEM (250 µl, Invitrogen) for 10 minutes, then added dropwise to the iPSCs. Selection with puromycin (1µg/ml) in StemFlex medium started 24-48 hours after transfection and continued for approximately 10 days until stable colonies formed. Individual colonies were picked with a P200 pipette tip under a microscope. Heterozygous and homozygous ADNP p.Tyr719-HA* iPSC clones, as well as heterozygous ADNP-HA iPSC clones, were confirmed by PCR. The puromycin-resistance cassette was removed using Cre-recombinase.

To generate iPSCs with stable inducible ASCL1-DLX2 integration, we took advantage of a bi-directional tetracycline-inducible promoter via the PiggyBac transposon system, as previously described [105]. The iPSCs were transfected with the PB-TO-ASCL1-DLX2 plasmid and the EF1a-transposase vector at a 2:1 ratio using Lipofectamine™ Stem Transfection Reagent. Selection with puromycin started 24-48 hours post-transfection and continued for 2 weeks. Successfully modified human iPSCs harboring stable TO-ASCL1-DLX2 integration were either cryopreserved for future applications or directly differentiated into neuronal cells. PB-TO-ASCL1-DLX2 (Addgene plasmid # 182307) and EF1a-transposase plasmid were gifts from iPSC Neurodegenerative Disease Initiative (iNDI) & Michael Ward.

Research on human-derived samples was conducted according to protocols approved by the institutional review boards of the Icahn School of Medicine at Mount Sinai.

Lentivirus production

Infectious lentiviral particles were produced in HEK293T cells using the third-generation lentiviral packaging plasmids: pMD2.G (Addgene plasmid # 12259), pRSV-rev (Addgene plasmid #: 12253), and pMDLg/pRRE (Addgene plasmid #: 12251) [106]. Lentiviruses were produced in HEK293T cells using polyethylenimine (PEI), following established protocols [107]. The lentiviral supernatant was centrifuged at 1,000g for 5 minutes to remove cellular debris. Lentiviral particles were then ultra-centrifuged, resuspended overnight with gentle shaking in

DMEM, aliquoted, and stored at -80°C. Only virus preparations with >90% infection efficiency were used for experiments, as determined by GFP expression or antibiotic resistance.

Small molecule-mediated GABAergic neuron generation

Human PSCs were differentiated into cortical inhibitory neurons using an established protocol based on dual SMAD inhibition, WNT inhibition, and SHH activation,[42,43] with the following modifications. NKX2.1(GFP/w) cells were dissociated into single cells using Accutase and plated at 430,000 cells/cm² onto Geltrex-coated wells in KSR media (415 mL Knockout DMEM, 75 mL knockout serum replacement, 500 µL 2-mercaptoethanol, 5 mL NEAA, and 5 mL GlutaMAX) supplemented with 10 µM Y-27632. From days 1 to 10, the cells underwent daily complete medium changes with LDN193189 (100 nM), SB431542 (10 µM), and XAV939 (2 µM). During days 11 to 18, N2 medium supplemented with 1 µM Purmorphamine and 5 µM recombinant SHH was used to induce ventral identity. On day 32, NKX2.1-GFP cells were dissociated, collected via FACS, and replated with mouse glial cells. The cells were maintained in Neurobasal A media supplemented with 1×B27, 1×Glutamax, 1% fetal bovine serum, and 2-4 µM AraC and harvested on day 67 for further analyses.

TF-mediated induced GABAergic neuron generation

We used our established protocol to generate GABAergic neurons through lentiviral-mediated overexpression of ASCL1 and DLX2, as previously described [27]. Briefly, PSCs were transduced with FUW-TetO-Ascl1-T2A-puromycin, FUW-TetO-Dlx2-IRES-hygromycin, and FUW-rtTA lentiviruses. Twenty-four hours later, the medium was replaced by N2 media (1´N2 supplement, 1´NEAA in DMEM-F12 media) supplemented with 2 µg/mL doxycycline to induce transgene expression. The transduced cells were selected for three days by applying hygromycin (200 µg/mL) and puromycin (1 µg/mL). Subsequently, the media was replaced with N2 media containing 4 µM AraC for an additional three days. On day 8, GABAergic neurons were co-cultured with mouse glial cells at a density of 104,000 cells/cm^2 on Geltrex-coated plates. Two weeks post-transgene induction, doxycycline was withdrawn, and the culture was maintained in Neurobasal A media supplemented with 1´B27, 1´Glutamax, and 1% fetal bovine serum. Mature neurons were used for various assays on day 35 after co-culture.

To generate GABAergic neurons from PSC lines with stable inducible ASCL1-DLX2 integration, PSCs were dissociated using Accutase and plated at a density of 100,000 cells/cm^2 on GelTrex -coated plates in StemFlex Medium supplemented with Chroman1. The following day, the medium was replaced with N2 media containing 2 µg/mL Doxycycline to induce the expression of ASCL1 and DLX2. After three days, 4 µM AraC was added to the N2 media. On day 8, the

neurons were replated with mouse glial cells. All subsequent procedures followed the previously described protocol for generating GABAergic neurons using lentiviral vectors.

Patterned induced GABAergic neuron generation

PSC lines with stable inducible ASCL1-DLX2 integration were dissociated into single cells using Accutase and plated at 430,000 cells/cm² onto Geltrex-coated wells in KSR media supplemented with 2 μM Chroman1. From days 1 to 10, the cells underwent daily full medium changes with LDN193189 (100 nM), SB431542 (10 μM), and XAV939 (2 μM). Starting on day 11, N2 media supplemented with 2 μg/mL doxycycline and 10 μM DAPT (Tocris Bioscience, 2634) was used to induce ASCL1 and DLX2 expression and promote synchronized neural differentiation. Doxycycline was discontinued either 3 or 7 days later, and DAPT was removed after 7 days. Neurons were then dissociated and replated with mouse glial cells. Subsequent steps followed the established protocols used for other GABAergic neuron differentiation methods.

METHOD DETAILS

Primary mouse astrocytes

Mouse glial cultures were generated from cortical hemispheres at postnatal day 3 (P03). The cortices were incubated in 3 mL of 20 Units/mL Papain, 0.5 μM EDTA, and 1 μM CaCl2 in HBSS for 15 mins. After incubation, the tissues were manually dissociated by forceful trituration. The resulting cells were grown at 37°C with 5% CO_2 in DMEM media containing 1×NEAA, 1× sodium pyruvate, 10% Cytiva HyClone™ Cosmic Calf™ Serum (CCS), and 0.008% β-mercaptoethanol.

Transplantation and Brain Slice Preparation

Concentrated cell suspensions (~1 × 10^5 cells/μL) were loaded into beveled glass micropipettes (Drummond Scientific). Each recipient received two injections of 0.5 μL into the forebrain at coordinates 2.0 mm posterior, 1.0 mm lateral, and 1.5 mm ventral to the skin surface, targeting the periventricular region. Stereotaxic coordinates were zeroed anteriorly at the inner corner of the eye, laterally at the midpoint between the eyes, and vertically at the skin surface. Following injection, pups were placed on a heating pad until fully warmed and active, then returned to their mothers. Animals were maintained with the dam until weaning at postnatal day 21 (P21).

Acute brain slices were prepared from approximately 6-month-old mice. Animals were deeply anesthetized with Euthasol and decapitated. Brains were rapidly removed and immersed in ~0 ^{o}C aerated (95% O_2 and 5% CO_2) sucrose-based slicing solution containing (in mM): 213 sucrose, 2.5 KCl, 2 $MgSO_4$, 2 $CaCl_2$, 26 $NaHCO_3$, 1.25 NaH_2PO_4, and 25 dextrose (315 mOsm, pH 7.4). In this slicing solution, coronal slices with a thickness of 300 mm were cut using a

vibratome (Leica VT1200S). Slices were cut from both female and male mouse brain and then incubated in aerated artificial cerebrospinal fluid (ACSF) containing (in mM): NaCl 126, KCl 2.5, NaH_2PO_4 1.25, $NaHCO_3$ 26, dextrose 25, $MgSO_4$ 2 and $CaCl_2$ 2 (315 mOsm, pH 7.4) at ~34°C for 50 min and then maintained at room temperature until recording.

Electrophysiological Recordings from Brain Slices

Slices were transferred to a recording chamber and perfused with oxygenated ACSF at 25°C. Human interneurons located in subcortical regions were visualized using an infrared differential interference contrast (IR-DIC) microscope (BX51WI, Olympus) equipped with a 40× water-immersion objective. Images were captured with a CMOS camera (C11440-36U, Hamamatsu) and displayed in real time. GFP-expressing human neurons were identified using 470-nm LED excitation. To assess intrinsic membrane properties, whole-cell current-clamp recordings were performed using 500-ms current steps of increasing amplitude. Patch pipettes (~5 MΩ) were filled with a K-gluconate–based internal solution containing (in mM): 140 K-Gluconate, 3 KCl, 2 $MgCl_2$, 0.2 EGTA, 10 HEPES and 2 Na_2ATP (287 mOsm, pH 7.22), supplemented with 0.2% biocytin for post hoc morphological analysis. Voltage signals were filtered at 10 kHz and sampled at 40 kHz, while synaptic currents were low-pass filtered at 3 kHz and sampled at 40 kHz using a Multiclamp 700B amplifier and Clampex 11.2 software (Molecular Devices).

Whole-cell recordings from cultured neurons

Functional properties of iNs were assessed using whole-cell patch-clamp electrophysiology as previously described.[27,30] Spontaneous inhibitory postsynaptic currents (sIPSCs) were recorded at a holding potential of −70 mV in the presence of 20 μM CNQX. Miniature inhibitory postsynaptic currents (mIPSCs) were recorded at −70 mV in the presence of 1 μM tetrodotoxin (TTX) and 20 μM CNQX. Patch pipettes were filled with a Cs-based internal solution containing (in mM): 40 CsCl, 3.5 KCl, 10 HEPES, 0.05 EGTA, 90 K-gluconate, 1.8 NaCl, 1.7 $MgCl_2$, 2 Mg-ATP, 0.4 Na-GTP, and 10 phosphocreatine. The external recording solution contained (in mM): 140 NaCl, 5 KCl, 10 HEPES, 2 $CaCl_2$, 2 $MgCl_2$, and 10 glucose (pH 7.4). All recordings were performed at room temperature.

Immunofluorescence and imaging

Cultured cells were fixed with 4% paraformaldehyde in D-PBS at room temperature for 5-10 min. Cells were rinsed 3 times with D-PBS and subsequently permeabilized for 5 mins at room temperature with 0.2% Triton X-100 in D-PBS. After incubation in blocking buffer (4% bovine serum albumin (BSA) and 1% Cosmic Calf™ Serum in D-PBS) for 3 hours, primary antibodies were added for incubation overnight at 4°C. After 3 rinses, cells were incubated with secondary

antibodies in the blocking buffer for 3 h at room temperature. Images were acquired using the EVOS M5000 imaging system (Life Technologies).

Images of injected human neurons in mouse brain sections were acquired at the Microscopy and Advanced Bioimaging CoRE at the Icahn School of Medicine at Mount Sinai. Imaging was performed using ZEN Blue software (v3.7.4) on a Zeiss LSM980 confocal microscope equipped with a 32-channel Airyscan 2 GaAsP-PMT detector, operated in super-resolution (SR) mode with Multiplex 4Y. Images were collected using a 100×/1.46 NA α-Plan-Apochromat oil-immersion objective with a minimum optical zoom of 1.7. Frame size was set to “optimal” to ensure Nyquist sampling for the selected field of view. Images were acquired at 16-bit depth, with scan speed set to “maximum” and a frame average of 1. Excitation was provided by an argon 488-nm laser for GFP and a 561-nm diode laser for Alexa Fluor 561. Emission was collected using a main beam splitter (MBS) 488/561, a secondary beam splitter (SBS) SP615, and dual emission filters (BP 420–480 and BP 495–550 for GFP; BP 570–620 and LP645 for Alexa Fluor 561). For z-stack acquisition, the z-step size was set to half of the axial resolution (0.4 µm per step) to ensure adequate sampling. For each experimental cohort, positive control samples were used to establish excitation and detection parameters, including laser power and detector gain. Settings were optimized to maximize signal-to-noise ratio while using approximately 50% of the detector’s dynamic range and avoiding saturation. Detector gain was maintained below 850 V to ensure linear response, and laser power rarely exceeded 1%. Once established, these parameters were held constant for all samples within each cohort. Image processing was performed using the ZEN Airyscan processing module.

Immunoblotting

Cells were washed three times with cold PBS, harvested using CELLTREAT cell lifters, and lysed with the RIPA Lysis and Extraction Buffer (supplemented with 1X Halt Protease and Phosphatase Inhibitor Cocktail and 5 mM EDTA). Cells were incubated on ice for 15 min with occasional vortexing, sonicated twice (1s pulse followed by 1 min on ice), incubated on ice for another 15 min with occasional vortexing, and then centrifuged at 21000 xg for 20 min with the supernatant collected for quantifications using the BCA assay. Samples were denatured with 1X NuPAGE LDS loading buffer (supplemented with 50 mM DTT) and incubated at 70 ºC for 10 min.

Approximately 25 µg of total proteins were loaded onto each well of the 4-12% Bis-Tris gel and run at 170 V for 30 min in 1X MOPS Buffer. Samples were then transferred onto PVDF membrane at 20 V for 1 h at 4 ºC in cold 1X Transfer Buffer (25 mM Tris, 200 mM Glycine, 15%

MeOH in ddH2O), blocked with either the LICOR Blocking Buffer or 5% milk in TBST for 1h at RT, then incubated overnight at 4ºC on the rocking shaker with the addition of primary antibodies diluted in the corresponding blocking buffer supplemented with 0.1% Tween-20. Membranes were washed four times with TBST (5 min at RT on the shaker each time), incubated at RT for 1h with secondary antibodies (diluted in the corresponding blocking buffer and supplemented with 0.1% Tween-20 and 0.1% SDS), washed for another 4 times with TBST (for HRP antibodies, treated with the ECL buffer at A:B = 1:1 in dark for 5 min at RT before imaging), and imaged using the Bio-Rad ChemiDoc MP Imaging System.

10X single-cell RNA-seq library preparation and sequencing

We used a Papain solution to create single-cell suspensions based on a published method.[108] Neurons were detached from the plate using Accutase supplemented with 0.4% DNase (Worthington), collected and further dissociated with a Papain solution. This solution was prepared by adding 328 µL of Papain to each 20 mL Enzyme Stock Solution containing 1× EBSS, 0.46% D(+) Glucose, 26 mM NaHCO3, and 0.5 mM EDTA. Additionally, 0.004 g of L-cysteine was added before use. The solution was activated for 15 minutes at 37°C, followed by an additional 1.5-hour incubation at 37°C. Prepare the Inhibitor Stock Solution (0.46% D(+) Glucose and 25 mM NaHCO3 in1× EBSS), Low Ovo (10X) solution (3 g BSA (Sigma A8806), and 3 g Trypsin inhibitor (Worthington LS003086) in 200 mL D-PBS, adjusting the pH to 7.4) and High Ovo (5X) solution (6 g BSA and 6 g Trypsin inhibitor in 200 mL D-PBS, pH 7.4). The single-cell suspension was washed four times, alternating between low Ovo solution (9 mL inhibitor stock solution and 1 mL Low Ovo (10X)) and high Ovo solution (4 mL inhibitor stock solution and 1 mL High Ovo (5X)). After washing, the cells were centrifuged at 350 g for 5 minutes, and the resulting cell pellet was resuspended in cold 0.02% BSA. Single-cell RNA sequencing library preparation was performed using the Chromium Single Cell 3’ Reagent V3 kit, following the manufacturer’s specifications. Barcoded libraries were sequenced on the Illumina NovaSeq platform with 150 bp paired-end reads, achieving an average depth of approximately 30,000 reads per cell.

SHARE-seq library preparation and sequencing

SHARE-seq libraries were prepared as previously described[67]. Briefly, cells were fixed using 0.2% formaldehyde and permeabilized. For joint measurements of single-cell chromatin accessibility and expression (scATAC- and scRNA-seq), cells were first transposed by Tn5 transposase to mark regions of open chromatin. The mRNA was reverse transcribed using a poly(T) primer containing a unique molecular identifier (UMI) and a biotin tag. Permeabilized cells were distributed in a 96-well plate to hybridize well-specific barcoded oligonucleotides to transposed

chromatin fragments and poly(T) cDNA. Hybridization was repeated three times to expand the barcoding space and ligate cell barcodes to cDNA and chromatin fragments. Reverse crosslinking was performed to release barcoded molecules. cDNA was separated from chromatin using streptavidin beads, and each library was prepared separately for sequencing. Libraries were sequenced on the Illumina NovaSeq platform (read 1: 50 cycles, read 2: 50 cycles, index 1: 99 cycles, index 2: 8 cycles).

QUANTIFICATION AND STATISTICAL ANALYSIS

10X Single-cell RNA-sequencing data processing and analysis

All single-cell RNA sequencing (scRNA-seq) samples were processed individually. Sequencing reads were aligned to a combined GRCh38 human and mm10 mouse reference transcriptomes (GRCh38_and_mm10-2020-A) using Cellranger (v7.0) with default parameters to generate gene-by-cell count matrices. Downstream analyses were performed in R using Seurat (v5.0.1). The data was filtered to retain only genes annotated to the human genome, and features were retained if detected in at least 3 cells and with a minimum of 200 features per cell. High-quality cells were selected based on having 500 to 7,000 detected genes and a maximum of 20% of reads mapping to mitochondrial genes. For 7D-patterned neurons and ADNP neuron samples, doublets were removed using DoubletFinder (v2.0) with default parameters. After preprocessing, samples were merged and normalized using natural-log transformation, and counts were scaled by a factor of 10,000. Principal component analysis (PCA) was conducted on the 2,000 most variable features (FindVariableFeatures()). The first 20 principal components (k=20) were used to construct a K-nearest neighbor (KNN) graph, while the first 30 principal components were used for ADNP samples. Cells were clustered using the Louvain algorithm (FindClusters()) and visualized using UMAP embeddings. Clusters were manually annotated with cell types based on a curated list of markers (Table S2). When necessary, samples were integrated using the FastMNN algorithm (IntegrateLayers()). After merging or integration, genes related to the cell cycle and ribosomal function were regressed out. Differential expression analysis between clusters or samples was performed using the Wilcoxon rank sum test using only genes expressed by a minimum of 3-5% of cells. Method/cluster specificity genes were identified as previously described [109]. Briefly, genes with non-unique names or not expressed in any cells were filtered out. Gene expression was scaled to 1 million unique molecular identifiers per method or cluster. Gene expression specificity was calculated by dividing the expression of each gene in each method/cluster by the total expression of all genes in that method/cluster, resulting in values from 0 to 1, with values closer to 1 indicating high specificity. The top 10% of

the most highly specific genes per method or cluster were used for gene expression analyses. Pseudotime trajectory analysis was performed using Slingshot (v2.7.0) or Monocle3 (v.1.3.7) software with default parameters. Graphtest() in Monocle3 was used to determine genes that change with pseudotime.

To assess the similarity of PSC-derived GABAergic neurons to inhibitory neurons from different regions of the developing fetal brain, we utilized previously published scRNA-seq data from Bhaduri et al. [53] encompassing weeks 18, 19, 20, and 25 of gestation across various brain regions (neocortex, striatum, thalamus, hypothalamus, ganglionic eminence, midbrain, and cerebellum). Additionally, hypothalamic neuron data from Herb et al. [54] were included. All datasets were merged into a single Seurat object for comprehensive analysis. The combined dataset was first refined to focus on neurons expressing the inhibitory neuron makers GAD1/2 (log norm counts > 0). We employed Seurat's FindTransferAnchors() and MapQuery() functions for cell mapping and comparison. The data normalization was carried out using SCTransform.

To compare cell states across differentiation approaches, publicly available scRNA-seq datasets were independently reprocessed using Seurat. Gene-by-cell count matrices were log-normalized and scaled, and the top 2,000 highly variable genes were selected for dimensionality reduction. Principal component analysis (PCA) was performed using 50 components, followed by UMAP embedding (min.dist = 0.3). To assign lineage and cell-state identities, each dataset was mapped onto a reference atlas of the developing human brain.[49] The reference dataset was processed using the same pipeline, except that 20 principal components were used for UMAP construction. Anchor-based mapping was performed using FindTransferAnchors() (reduction = "rpca", k.anchor = 20), followed by cell-type annotation with TransferData() (dims = 1:20, k.weight = 10). This strategy enabled consistent assignment of interneuron lineage and regional identities across differentiation methods.

SHARE-seq data processing and analysis

SHARE-seq libraries were aligned using a published pipeline (https://github.com/masai1116/SHARE-seq-alignmentV2). Briefly, sequencing reads were trimmed and aligned to the hg38 genome using Bowtie2. Reads were demultiplexed using four sets of 8-bp barcodes in the index reads, allowing one mismatch per barcode. Reads mapping to the mitochondria and chrY were discarded. Duplicates were removed based on the read alignment position and cell barcodes. Open chromatin region peaks were called on merged samples using MACS2. Peaks overlapping with ENCODE blacklisted regions (https://sites.google.com/site/anshulkundaje/projects/blacklists) were filtered out. Peak summits were extended by 250bp on each side and defined as accessible regions. The fragment counts

in peaks and TF scores were calculated using chromVAR. SHARE-RNA-seq reads were aligned to the hg38 genome using STAR. Reads were demultiplexed as described above for SHARE-ATAC-seq. Aligned reads were annotated to both exons and introns using feature counts. PCR duplicates were removed based on UMIs and read alignment position. Cells that expressed >1,000 genes and <4% mitochondrial reads were retained. Seurat was used to preprocess the count matrix and cluster cells for scRNA-seq libraries as described above. For pseudotime trajectory analysis, hPSCs, NPC-like cells, and stressed cells were removed, and Slingshot was utilized with default parameters.

Inferring regulatory networks

To infer transcription factor (TF) regulon networks within our single-cell RNA-seq dataset, we utilized the SCENIC (Single-Cell Regulatory Network Inference and Clustering) [61] protocol (v1.1.2), which employs the vsn-pipeline version orchestrated via Nextflow with the pyscenic (v0.12.1) container. First, Seurat objects were converted into loom files using the SCopeLoomR package (v0.13.0). Subsequently, the pyscenic module was executed 20 times using its default settings. Only regulons identified in at least 15 out of the 20 runs were included for further analysis.

Gene Ontology, pathway enrichment and disease-vulnerable cell type analysis

We used Enrichr [110] or ClusterProfiler (with universe set to all expressed genes in dataset to identify the cellular functions and biological processes of differentially expressed genes. To identify the cellular functions of differential peaks, we annotated the peaks to their nearest genes, followed by Enrichr analysis.

To determine the enrichment of genes implicated in autism spectrum disorder (ASD), we used the Simons Foundation Autism Research Initiative (SFARI) database to compile a list of 1,065 ASD-associated genes scored 0-2 or categorized as syndromic. Fisher's exact test was performed to determine the statistical significance of the top 10% of differentially expressed genes specific to PSC-iGABAs or patterned-iGABAs.

For a more comprehensive analysis of all neural-related diseases, we used the ToppGene Suite and selected the DisGeNET Curated database,[57] which includes a total of 11,181 annotations. DisGeNET integrates information on gene-disease associations from repositories, GWAS catalogs, animal models, and scientific literature. To control for multiple testing errors, a threshold of 0.05 was applied. We used a random sampling size of 5,000, considering only coding genes to ensure the results were not biased by the size of the gene list, and required a minimum feature count of at least two genes in our DEG list. Only disease associations with an

FDR-adjusted p-value ≤ 0.05 (Benjamini-Hochberg for multiple hypothesis testing) were considered significant.

To assess disease vulnerability across neurons generated using our differentiation approaches, we integrated our scRNA-seq data with publicly available reference datasets from postmortem human brain tissue. Specifically, we used datasets from individuals with AD[59] and ASD[60], which define interneuron populations reported to exhibit selective vulnerability in each disease context. Using a reference-mapping framework, we projected cells from these datasets onto our induced GABAergic neuron atlas. We then quantified the fraction of cells generated by each differentiation strategy that mapped to disease-vulnerable cell types, enabling comparative assessment of how well each approach captures interneuron populations implicated in AD- and ASD-related pathology.

WGCNA analysis

A total of 8,516 genes with an average expression level above 0.15 were selected for WGCNA analysis.[111,112] To construct the network, a soft thresholding is selected through scale independence: power = 4 for clusters 0 and 2 and power = 3 for cluster 1. Gene clustering and module assignments were visualized using a dendrogram, highlighting the hierarchical relationships between gene modules.

Statistical analyses

Unless otherwise indicated, all data presented are the average of at least two biological replicates from each of at least two independent experiments. Statistical analysis was matched to the data structure as noted above in the Methods Details section for single-cell RNA-seq and SHARE-seq experiments. Statistical analyses were performed in RStudio (v4.3.1; RStudio team, 2020) or GraphPad Prism 9. See figure legends for details on specific statistical tests run for each experiment. Statistical significance is represented by a star (*) and indicates a computed P-value < 0.05. Graphs and plots were generated using Graphpad Prism or RStudio. Figures were generated using Adobe Illustrator and Biolegend.

REFERENCES

1. Le Magueresse, C., and Monyer, H. (2013). GABAergic interneurons shape the functional maturation of the cortex. Neuron *77*, 388-405. 10.1016/j.neuron.2013.01.011.
2. Wamsley, B., and Fishell, G. (2017). Genetic and activity-dependent mechanisms underlying interneuron diversity. Nat Rev Neurosci *18*, 299-309. 10.1038/nrn.2017.30.
3. Marin, O. (2012). Interneuron dysfunction in psychiatric disorders. Nat Rev Neurosci *13*, 107-120. 10.1038/nrn3155.
4. Verret, L., Mann, E.O., Hang, G.B., Barth, A.M., Cobos, I., Ho, K., Devidze, N., Masliah, E., Kreitzer, A.C., Mody, I., et al. (2012). Inhibitory interneuron deficit links altered network activity and cognitive dysfunction in Alzheimer model. Cell *149*, 708-721. 10.1016/j.cell.2012.02.046.
5. Xu, Q., Tam, M., and Anderson, S.A. (2008). Fate mapping Nkx2.1-lineage cells in the mouse telencephalon. J Comp Neurol *506*, 16-29. 10.1002/cne.21529.
6. Xu, Q., Cobos, I., De La Cruz, E., Rubenstein, J.L., and Anderson, S.A. (2004). Origins of cortical interneuron subtypes. J Neurosci *24*, 2612-2622. 10.1523/JNEUROSCI.5667-03.2004.
7. Wonders, C.P., and Anderson, S.A. (2006). The origin and specification of cortical interneurons. Nat Rev Neurosci *7*, 687-696. 10.1038/nrn1954.
8. Butt, S.J., Sousa, V.H., Fuccillo, M.V., Hjerling-Leffler, J., Miyoshi, G., Kimura, S., and Fishell, G. (2008). The requirement of Nkx2-1 in the temporal specification of cortical interneuron subtypes. Neuron *59*, 722-732. 10.1016/j.neuron.2008.07.031.
9. Bandler, R.C., and Mayer, C. (2023). Deciphering inhibitory neuron development: The paths to diversity. Curr Opin Neurobiol *79*, 102691. 10.1016/j.conb.2023.102691.
10. Yozu, M., Tabata, H., and Nakajima, K. (2005). The caudal migratory stream: a novel migratory stream of interneurons derived from the caudal ganglionic eminence in the developing mouse forebrain. J Neurosci *25*, 7268-7277. 10.1523/JNEUROSCI.2072-05.2005.
11. Nery, S., Fishell, G., and Corbin, J.G. (2002). The caudal ganglionic eminence is a source of distinct cortical and subcortical cell populations. Nat Neurosci *5*, 1279-1287. 10.1038/nn971.
12. Miyoshi, G., Hjerling-Leffler, J., Karayannis, T., Sousa, V.H., Butt, S.J., Battiste, J., Johnson, J.E., Machold, R.P., and Fishell, G. (2010). Genetic fate mapping reveals that the caudal ganglionic eminence produces a large and diverse population of superficial cortical interneurons. J Neurosci *30*, 1582-1594. 10.1523/JNEUROSCI.4515-09.2010.
13. Schmitz, M.T., Sandoval, K., Chen, C.P., Mostajo-Radji, M.A., Seeley, W.W., Nowakowski, T.J., Ye, C.J., Paredes, M.F., and Pollen, A.A. (2022). The development and evolution of inhibitory neurons in primate cerebrum. Nature *603*, 871-877. 10.1038/s41586-022-04510-w.
14. Li, Y., Li, Z., Wang, C., Yang, M., He, Z., Wang, F., Zhang, Y., Li, R., Gong, Y., Wang, B., et al. (2023). Spatiotemporal transcriptome atlas reveals the regional specification of the developing human brain. Cell *186*, 5892-5909 e5822. 10.1016/j.cell.2023.11.016.
15. Bozzi, Y., Casarosa, S., and Caleo, M. (2012). Epilepsy as a neurodevelopmental disorder. Front Psychiatry *3*, 19. 10.3389/fpsyt.2012.00019.
16. Inan, M., Petros, T.J., and Anderson, S.A. (2013). Losing your inhibition: linking cortical GABAergic interneurons to schizophrenia. Neurobiol Dis *53*, 36-48. 10.1016/j.nbd.2012.11.013.
17. Katsarou, A.M., Moshe, S.L., and Galanopoulou, A.S. (2017). Interneuronopathies and Their Role in Early Life Epilepsies and Neurodevelopmental Disorders. Epilepsia Open *2*, 284-306. 10.1002/epi4.12062.

18. Yu, Y., Zeng, Z., Xie, D., Chen, R., Sha, Y., Huang, S., Cai, W., Chen, W., Li, W., Ke, R., and Sun, T. (2021). Interneuron origin and molecular diversity in the human fetal brain. Nat Neurosci *24*, 1745-1756. 10.1038/s41593-021-00940-3.
19. Krienen, F.M., Goldman, M., Zhang, Q., R, C.H.D.R., Florio, M., Machold, R., Saunders, A., Levandowski, K., Zaniewski, H., Schuman, B., et al. (2020). Innovations present in the primate interneuron repertoire. Nature *586*, 262-269. 10.1038/s41586-020-2781-z.
20. Molnar, Z., Clowry, G.J., Sestan, N., Alzu'bi, A., Bakken, T., Hevner, R.F., Huppi, P.S., Kostovic, I., Rakic, P., Anton, E.S., et al. (2019). New insights into the development of the human cerebral cortex. J Anat *235*, 432-451. 10.1111/joa.13055.
21. Hladnik, A., Dzaja, D., Darmopil, S., Jovanov-Milosevic, N., and Petanjek, Z. (2014). Spatio-temporal extension in site of origin for cortical calretinin neurons in primates. Front Neuroanat *8*, 50. 10.3389/fnana.2014.00050.
22. Hansen, D.V., Lui, J.H., Flandin, P., Yoshikawa, K., Rubenstein, J.L., Alvarez-Buylla, A., and Kriegstein, A.R. (2013). Non-epithelial stem cells and cortical interneuron production in the human ganglionic eminences. Nat Neurosci *16*, 1576-1587. 10.1038/nn.3541.
23. Goff, K.M., and Goldberg, E.M. (2021). A Role for Vasoactive Intestinal Peptide Interneurons in Neurodevelopmental Disorders. Dev Neurosci *43*, 168-180. 10.1159/000515264.
24. Herrlinger, S.A., Wang, J., Rao, B.Y., Chang, J., Gogos, J.A., Losonczy, A., and Vitkup, D. (2025). Rare mutations implicate CGE interneurons as a vulnerable axis of cognitive deficits across psychiatric disorders. bioRxiv. 10.1101/2025.03.28.645799.
25. Skene, N.G., Bryois, J., Bakken, T.E., Breen, G., Crowley, J.J., Gaspar, H.A., Giusti-Rodriguez, P., Hodge, R.D., Miller, J.A., Munoz-Manchado, A.B., et al. (2018). Genetic identification of brain cell types underlying schizophrenia. Nat Genet *50*, 825-833. 10.1038/s41588-018-0129-5.
26. Eichmuller, O.L., Corsini, N.S., Vertesy, A., Morassut, I., Scholl, T., Gruber, V.E., Peer, A.M., Chu, J., Novatchkova, M., Hainfellner, J.A., et al. (2022). Amplification of human interneuron progenitors promotes brain tumors and neurological defects. Science *375*, eabf5546. 10.1126/science.abf5546.
27. Yang, N., Chanda, S., Marro, S., Ng, Y.H., Janas, J.A., Haag, D., Ang, C.E., Tang, Y., Flores, Q., Mall, M., et al. (2017). Generation of pure GABAergic neurons by transcription factor programming. Nat Methods *14*, 621-628. 10.1038/nmeth.4291.
28. Hester, M.E., Murtha, M.J., Song, S., Rao, M., Miranda, C.J., Meyer, K., Tian, J., Boulting, G., Schaffer, D.V., Zhu, M.X., et al. (2011). Rapid and efficient generation of functional motor neurons from human pluripotent stem cells using gene delivered transcription factor codes. Mol Ther *19*, 1905-1912. 10.1038/mt.2011.135.
29. Zhang, Y., Pak, C., Han, Y., Ahlenius, H., Zhang, Z., Chanda, S., Marro, S., Patzke, C., Acuna, C., Covy, J., et al. (2013). Rapid single-step induction of functional neurons from human pluripotent stem cells. Neuron *78*, 785-798. 10.1016/j.neuron.2013.05.029.
30. Pang, Z.P., Yang, N., Vierbuchen, T., Ostermeier, A., Fuentes, D.R., Yang, T.Q., Citri, A., Sebastiano, V., Marro, S., Sudhof, T.C., and Wernig, M. (2011). Induction of human neuronal cells by defined transcription factors. Nature *476*, 220-223. 10.1038/nature10202.
31. Chanda, S., Ang, C.E., Davila, J., Pak, C., Mall, M., Lee, Q.Y., Ahlenius, H., Jung, S.W., Sudhof, T.C., and Wernig, M. (2014). Generation of induced neuronal cells by the single reprogramming factor ASCL1. Stem Cell Reports *3*, 282-296. 10.1016/j.stemcr.2014.05.020.
32. Limone, F., Guerra San Juan, I., Mitchell, J.M., Smith, J.L.M., Raghunathan, K., Meyer, D., Ghosh, S.D., Couto, A., Klim, J.R., Joseph, B.J., et al. (2023). Efficient generation of lower induced motor neurons by coupling Ngn2 expression with developmental cues. Cell Rep *42*, 111896. 10.1016/j.celrep.2022.111896.

33. Nehme, R., Zuccaro, E., Ghosh, S.D., Li, C., Sherwood, J.L., Pietilainen, O., Barrett, L.E., Limone, F., Worringer, K.A., Kommineni, S., et al. (2018). Combining NGN2 Programming with Developmental Patterning Generates Human Excitatory Neurons with NMDAR-Mediated Synaptic Transmission. Cell Rep *23*, 2509-2523. 10.1016/j.celrep.2018.04.066.
34. Sanchez-Priego, C., Hu, R., Boshans, L.L., Lalli, M., Janas, J.A., Williams, S.E., Dong, Z., and Yang, N. (2022). Mapping cis-regulatory elements in human neurons links psychiatric disease heritability and activity-regulated transcriptional programs. Cell Rep *39*, 110877. 10.1016/j.celrep.2022.110877.
35. Marro, S.G., Chanda, S., Yang, N., Janas, J.A., Valperga, G., Trotter, J., Zhou, B., Merrill, S., Yousif, I., Shelby, H., et al. (2019). Neuroligin-4 Regulates Excitatory Synaptic Transmission in Human Neurons. Neuron *103*, 617-626 e616. 10.1016/j.neuron.2019.05.043.
36. Chambers, S.M., Qi, Y., Mica, Y., Lee, G., Zhang, X.J., Niu, L., Bilsland, J., Cao, L., Stevens, E., Whiting, P., et al. (2012). Combined small-molecule inhibition accelerates developmental timing and converts human pluripotent stem cells into nociceptors. Nat Biotechnol *30*, 715-720. 10.1038/nbt.2249.
37. Fu, J.M., Satterstrom, F.K., Peng, M., Brand, H., Collins, R.L., Dong, S., Wamsley, B., Klei, L., Wang, L., Hao, S.P., et al. (2022). Rare coding variation provides insight into the genetic architecture and phenotypic context of autism. Nat Genet *54*, 1320-1331. 10.1038/s41588-022-01104-0.
38. Graf, T., and Enver, T. (2009). Forcing cells to change lineages. Nature *462*, 587-594. 10.1038/nature08533.
39. Wang, H., Yang, Y., Liu, J., and Qian, L. (2021). Direct cell reprogramming: approaches, mechanisms and progress. Nat Rev Mol Cell Biol *22*, 410-424. 10.1038/s41580-021-00335-z.
40. English, J., McSweeney, D., Ribbe, F., Howell, E., and Pak, C. (2023). Generation and Co-culture of Cortical Glutamatergic and GABAergic-Induced Neuronal Cells. Methods Mol Biol *2683*, 21-37. 10.1007/978-1-0716-3287-1_3.
41. Gonzalez-Ramos, A., Waloschkova, E., Mikroulis, A., Kokaia, Z., Bengzon, J., Ledri, M., Andersson, M., and Kokaia, M. (2021). Human stem cell-derived GABAergic neurons functionally integrate into human neuronal networks. Sci Rep *11*, 22050. 10.1038/s41598-021-01270-x.
42. Maroof, A.M., Keros, S., Tyson, J.A., Ying, S.W., Ganat, Y.M., Merkle, F.T., Liu, B., Goulburn, A., Stanley, E.G., Elefanty, A.G., et al. (2013). Directed differentiation and functional maturation of cortical interneurons from human embryonic stem cells. Cell Stem Cell *12*, 559-572. 10.1016/j.stem.2013.04.008.
43. Nicholas, C.R., Chen, J., Tang, Y., Southwell, D.G., Chalmers, N., Vogt, D., Arnold, C.M., Chen, Y.J., Stanley, E.G., Elefanty, A.G., et al. (2013). Functional maturation of hPSC-derived forebrain interneurons requires an extended timeline and mimics human neural development. Cell Stem Cell *12*, 573-586. 10.1016/j.stem.2013.04.005.
44. Liu, Y., Liu, H., Sauvey, C., Yao, L., Zarnowska, E.D., and Zhang, S.C. (2013). Directed differentiation of forebrain GABA interneurons from human pluripotent stem cells. Nat Protoc *8*, 1670-1679. 10.1038/nprot.2013.106.
45. Schill, D.J., Attili, D., DeLong, C.J., McInnis, M.G., Johnson, C.N., Murphy, G.G., and O'Shea, K.S. (2024). Human-Induced Pluripotent Stem Cell (iPSC)-Derived GABAergic Neuron Differentiation in Bipolar Disorder. Cells *13*. 10.3390/cells13141194.
46. Ciceri, G., Baggiolini, A., Cho, H.S., Kshirsagar, M., Benito-Kwiecinski, S., Walsh, R.M., Aromolaran, K.A., Gonzalez-Hernandez, A.J., Munguba, H., Koo, S.Y., et al. (2024). An epigenetic barrier sets the timing of human neuronal maturation. Nature *626*, 881-890. 10.1038/s41586-023-06984-8.

47. Lin, Y., Yang, J., Shen, Z., Ma, J., Simons, B.D., and Shi, S.H. (2021). Behavior and lineage progression of neural progenitors in the mammalian cortex. Curr Opin Neurobiol *66*, 144-157. 10.1016/j.conb.2020.10.017.
48. Shi, Y., Wang, M., Mi, D., Lu, T., Wang, B., Dong, H., Zhong, S., Chen, Y., Sun, L., Zhou, X., et al. (2021). Mouse and human share conserved transcriptional programs for interneuron development. Science *374*, eabj6641. 10.1126/science.abj6641.
49. Feng, X., Gao, Y., Chu, F., Shan, Y., Liu, M., Wang, Y., Zhu, Y., Lu, Q., and Li, M. (2025). Cortical arealization of interneurons defines shared and distinct molecular programs in developing human and macaque brains. Nat Commun *16*, 672. 10.1038/s41467-025-56058-8.
50. Kim, D.W., Place, E., Chinnaiya, K., Manning, E., Sun, C., Dai, W., Groves, I., Ohyama, K., Burbridge, S., Placzek, M., and Blackshaw, S. (2022). Single-cell analysis of early chick hypothalamic development reveals that hypothalamic cells are induced from prethalamic-like progenitors. Cell Rep *38*, 110251. 10.1016/j.celrep.2021.110251.
51. Kim, D.W., Liu, K., Wang, Z.Q., Zhang, Y.S., Bathini, A., Brown, M.P., Lin, S.H., Washington, P.W., Sun, C., Lindtner, S., et al. (2021). Gene regulatory networks controlling differentiation, survival, and diversification of hypothalamic Lhx6-expressing GABAergic neurons. Commun Biol *4*, 95. 10.1038/s42003-020-01616-7.
52. Traynelis, S.F., Wollmuth, L.P., McBain, C.J., Menniti, F.S., Vance, K.M., Ogden, K.K., Hansen, K.B., Yuan, H., Myers, S.J., and Dingledine, R. (2010). Glutamate receptor ion channels: structure, regulation, and function. Pharmacol Rev *62*, 405-496. 10.1124/pr.109.002451.
53. Bhaduri, A., Sandoval-Espinosa, C., Otero-Garcia, M., Oh, I., Yin, R., Eze, U.C., Nowakowski, T.J., and Kriegstein, A.R. (2021). An atlas of cortical arealization identifies dynamic molecular signatures. Nature *598*, 200-204. 10.1038/s41586-021-03910-8.
54. Herb, B.R., Glover, H.J., Bhaduri, A., Colantuoni, C., Bale, T.L., Siletti, K., Hodge, R., Lein, E., Kriegstein, A.R., Doege, C.A., and Ament, S.A. (2023). Single-cell genomics reveals region-specific developmental trajectories underlying neuronal diversity in the human hypothalamus. Sci Adv *9*, eadf6251. 10.1126/sciadv.adf6251.
55. Silva, J.P., von Meyenn, F., Howell, J., Thorens, B., Wolfrum, C., and Stoffel, M. (2009). Regulation of adaptive behaviour during fasting by hypothalamic Foxa2. Nature *462*, 646-650. 10.1038/nature08589.
56. Close, J.L., Yao, Z., Levi, B.P., Miller, J.A., Bakken, T.E., Menon, V., Ting, J.T., Wall, A., Krostag, A.R., Thomsen, E.R., et al. (2017). Single-Cell Profiling of an In Vitro Model of Human Interneuron Development Reveals Temporal Dynamics of Cell Type Production and Maturation. Neuron *93*, 1035-1048 e1035. 10.1016/j.neuron.2017.02.014.
57. Pinero, J., Ramirez-Anguita, J.M., Sauch-Pitarch, J., Ronzano, F., Centeno, E., Sanz, F., and Furlong, L.I. (2020). The DisGeNET knowledge platform for disease genomics: 2019 update. Nucleic Acids Res *48*, D845-D855. 10.1093/nar/gkz1021.
58. Abrahams, B.S., Arking, D.E., Campbell, D.B., Mefford, H.C., Morrow, E.M., Weiss, L.A., Menashe, I., Wadkins, T., Banerjee-Basu, S., and Packer, A. (2013). SFARI Gene 2.0: a community-driven knowledgebase for the autism spectrum disorders (ASDs). Mol Autism *4*, 36. 10.1186/2040-2392-4-36.
59. Gabitto, M.I., Travaglini, K.J., Rachleff, V.M., Kaplan, E.S., Long, B., Ariza, J., Ding, Y., Mahoney, J.T., Dee, N., Goldy, J., et al. (2024). Integrated multimodal cell atlas of Alzheimer's disease. Nat Neurosci *27*, 2366-2383. 10.1038/s41593-024-01774-5.
60. Velmeshev, D., Perez, Y., Yan, Z., Valencia, J.E., Castaneda-Castellanos, D.R., Wang, L., Schirmer, L., Mayer, S., Wick, B., Wang, S., et al. (2023). Single-cell analysis of prenatal and postnatal human cortical development. Science *382*, eadf0834. 10.1126/science.adf0834.

61. Aibar, S., Gonzalez-Blas, C.B., Moerman, T., Huynh-Thu, V.A., Imrichova, H., Hulselmans, G., Rambow, F., Marine, J.C., Geurts, P., Aerts, J., et al. (2017). SCENIC: single-cell regulatory network inference and clustering. Nat Methods *14*, 1083-1086. 10.1038/nmeth.4463.
62. Hu, J.S., Vogt, D., Lindtner, S., Sandberg, M., Silberberg, S.N., and Rubenstein, J.L.R. (2017). Coup-TF1 and Coup-TF2 control subtype and laminar identity of MGE-derived neocortical interneurons. Development *144*, 2837-2851. 10.1242/dev.150664.
63. Zhou, X., Liu, F., Tian, M., Xu, Z., Liang, Q., Wang, C., Li, J., Liu, Z., Tang, K., He, M., and Yang, Z. (2015). Transcription factors COUP-TFI and COUP-TFII are required for the production of granule cells in the mouse olfactory bulb. Development *142*, 1593-1605. 10.1242/dev.115279.
64. Rodriguez-Zas, S.L., Southey, N.L., Rund, L., Antonson, A.M., Nowak, R.A., and Johnson, R.W. (2023). Prenatal and postnatal challenges affect the hypothalamic molecular pathways that regulate hormonal levels. PLoS One *18*, e0292952. 10.1371/journal.pone.0292952.
65. Fragkouli, A., van Wijk, N.V., Lopes, R., Kessaris, N., and Pachnis, V. (2009). LIM homeodomain transcription factor-dependent specification of bipotential MGE progenitors into cholinergic and GABAergic striatal interneurons. Development *136*, 3841-3851. 10.1242/dev.038083.
66. Su, Z., Wang, Z., Lindtner, S., Yang, L., Shang, Z., Tian, Y., Guo, R., You, Y., Zhou, W., Rubenstein, J.L., et al. (2022). Dlx1/2-dependent expression of Meis2 promotes neuronal fate determination in the mammalian striatum. Development *149*. 10.1242/dev.200035.
67. Ma, S., Zhang, B., LaFave, L.M., Earl, A.S., Chiang, Z., Hu, Y., Ding, J., Brack, A., Kartha, V.K., Tay, T., et al. (2020). Chromatin Potential Identified by Shared Single-Cell Profiling of RNA and Chromatin. Cell *183*, 1103-1116 e1120. 10.1016/j.cell.2020.09.056.
68. Barber, M., Andrews, W.D., Memi, F., Gardener, P., Ciantar, D., Tata, M., Ruhrberg, C., and Parnavelas, J.G. (2018). Vascular-Derived Vegfa Promotes Cortical Interneuron Migration and Proximity to the Vasculature in the Developing Forebrain. Cereb Cortex *28*, 2577-2593. 10.1093/cercor/bhy082.
69. Harrison-Uy, S.J., and Pleasure, S.J. (2012). Wnt signaling and forebrain development. Cold Spring Harb Perspect Biol *4*, a008094. 10.1101/cshperspect.a008094.
70. Okabe, K., Fukada, H., Tai-Nagara, I., Ando, T., Honda, T., Nakajima, K., Takeda, N., Fong, G.H., Ema, M., and Kubota, Y. (2020). Neuron-derived VEGF contributes to cortical and hippocampal development independently of VEGFR1/2-mediated neurotrophism. Dev Biol *459*, 65-71. 10.1016/j.ydbio.2019.11.016.
71. Singh, A., Mahesh, A., Noack, F., Cardoso de Toledo, B., Calegari, F., and Tiwari, V.K. (2022). Tcf12 and NeuroD1 cooperatively drive neuronal migration during cortical development. Development *149*. 10.1242/dev.200250.
72. Watson, L.A., Wang, X., Elbert, A., Kernohan, K.D., Galjart, N., and Berube, N.G. (2014). Dual effect of CTCF loss on neuroprogenitor differentiation and survival. J Neurosci *34*, 2860-2870. 10.1523/JNEUROSCI.3769-13.2014.
73. Elbert, A., Vogt, D., Watson, A., Levy, M., Jiang, Y., Brule, E., Rowland, M.E., Rubenstein, J., and Berube, N.G. (2019). CTCF Governs the Identity and Migration of MGE-Derived Cortical Interneurons. J Neurosci *39*, 177-192. 10.1523/JNEUROSCI.3496-17.2018.
74. Yamakawa, H., Cheng, J., Penney, J., Gao, F., Rueda, R., Wang, J., Yamakawa, S., Kritskiy, O., Gjoneska, E., and Tsai, L.H. (2017). The Transcription Factor Sp3 Cooperates with HDAC2 to Regulate Synaptic Function and Plasticity in Neurons. Cell Rep *20*, 1319-1334. 10.1016/j.celrep.2017.07.044.

75. Liu, Z., Zhang, Z., Lindtner, S., Li, Z., Xu, Z., Wei, S., Liang, Q., Wen, Y., Tao, G., You, Y., et al. (2019). Sp9 Regulates Medial Ganglionic Eminence-Derived Cortical Interneuron Development. Cereb Cortex *29*, 2653-2667. 10.1093/cercor/bhy133.
76. Moore, D.L., Blackmore, M.G., Hu, Y., Kaestner, K.H., Bixby, J.L., Lemmon, V.P., and Goldberg, J.L. (2009). KLF family members regulate intrinsic axon regeneration ability. Science *326*, 298-301. 10.1126/science.1175737.
77. Laub, F., Aldabe, R., Friedrich, V., Jr., Ohnishi, S., Yoshida, T., and Ramirez, F. (2001). Developmental expression of mouse Kruppel-like transcription factor KLF7 suggests a potential role in neurogenesis. Dev Biol *233*, 305-318. 10.1006/dbio.2001.0243.
78. Qin, J., Wang, C., Zhu, Y., Su, T., Dong, L., Huang, Y., and Hao, K. (2021). Mga safeguards embryonic stem cells from acquiring extraembryonic endoderm fates. Sci Adv *7*. 10.1126/sciadv.abe5689.
79. Zhou, W., Gross, K.M., and Kuperwasser, C. (2019). Molecular regulation of Snai2 in development and disease. J Cell Sci *132*. 10.1242/jcs.235127.
80. Howard, J.M., Nuguid, J.M., Ngole, D., and Nguyen, H. (2014). Tcf3 expression marks both stem and progenitor cells in multiple epithelia. Development *141*, 3143-3152. 10.1242/dev.106989.
81. Schulte, D., and Geerts, D. (2019). MEIS transcription factors in development and disease. Development *146*. 10.1242/dev.174706.
82. Van Dijck, A., Vulto-van Silfhout, A.T., Cappuyns, E., van der Werf, I.M., Mancini, G.M., Tzschach, A., Bernier, R., Gozes, I., Eichler, E.E., Romano, C., et al. (2019). Clinical Presentation of a Complex Neurodevelopmental Disorder Caused by Mutations in ADNP. Biol Psychiat *85*, 287-297. 10.1016/j.biopsych.2018.02.1173.
83. Helsmoortel, C., Vulto-van Silfhout, A.T., Coe, B.P., Vandeweyer, G., Rooms, L., van den Ende, J., Schuurs-Hoeijmakers, J.H., Marcelis, C.L., Willemsen, M.H., Vissers, L.E., et al. (2014). A SWI/SNF-related autism syndrome caused by de novo mutations in ADNP. Nat Genet *46*, 380-384. 10.1038/ng.2899.
84. Breen, M.S., Garg, P., Tang, L., Mendonca, D., Levy, T., Barbosa, M., Arnett, A.B., Kurtz-Nelson, E., Agolini, E., Battaglia, A., et al. (2020). Episignatures Stratifying Helsmoortel-Van Der Aa Syndrome Show Modest Correlation with Phenotype. Am J Hum Genet *107*, 555-563. 10.1016/j.ajhg.2020.07.003.
85. Alcantara, S., Ruiz, M., D'Arcangelo, G., Ezan, F., de Lecea, L., Curran, T., Sotelo, C., and Soriano, E. (1998). Regional and cellular patterns of reelin mRNA expression in the forebrain of the developing and adult mouse. J Neurosci *18*, 7779-7799. 10.1523/JNEUROSCI.18-19-07779.1998.
86. Pesold, C., Impagnatiello, F., Pisu, M.G., Uzunov, D.P., Costa, E., Guidotti, A., and Caruncho, H.J. (1998). Reelin is preferentially expressed in neurons synthesizing gamma-aminobutyric acid in cortex and hippocampus of adult rats. Proc Natl Acad Sci U S A *95*, 3221-3226. 10.1073/pnas.95.6.3221.
87. Baran, Y., Bercovich, A., Sebe-Pedros, A., Lubling, Y., Giladi, A., Chomsky, E., Meir, Z., Hoichman, M., Lifshitz, A., and Tanay, A. (2019). MetaCell: analysis of single-cell RNA-seq data using K-nn graph partitions. Genome Biol *20*, 206. 10.1186/s13059-019-1812-2.
88. Delgado, R.N., Allen, D.E., Keefe, M.G., Mancia Leon, W.R., Ziffra, R.S., Crouch, E.E., Alvarez-Buylla, A., and Nowakowski, T.J. (2022). Individual human cortical progenitors can produce excitatory and inhibitory neurons. Nature *601*, 397-403. 10.1038/s41586-021-04230-7.
89. Ostapcuk, V., Mohn, F., Carl, S.H., Basters, A., Hess, D., Iesmantavicius, V., Lampersberger, L., Flemr, M., Pandey, A., Thoma, N.H., et al. (2018). Activity-dependent neuroprotective protein recruits HP1 and CHD4 to control lineage-specifying genes. Nature *557*, 739-743. 10.1038/s41586-018-0153-8.

90. Sun, X., Yu, W., Li, L., and Sun, Y. (2020). ADNP Controls Gene Expression Through Local Chromatin Architecture by Association With BRG1 and CHD4. Front Cell Dev Biol *8*, 553. 10.3389/fcell.2020.00553.
91. Cho, H., Yoo, T., Moon, H., Kang, H., Yang, Y., Kang, M., Yang, E., Lee, D., Hwang, D., Kim, H., et al. (2023). Adnp-mutant mice with cognitive inflexibility, CaMKIIalpha hyperactivity, and synaptic plasticity deficits. Mol Psychiatry *28*, 3548-3562. 10.1038/s41380-023-02129-5.
92. Bend, E.G., Aref-Eshghi, E., Everman, D.B., Rogers, R.C., Cathey, S.S., Prijoles, E.J., Lyons, M.J., Davis, H., Clarkson, K., Gripp, K.W., et al. (2019). Gene domain-specific DNA methylation episignatures highlight distinct molecular entities of ADNP syndrome. Clin Epigenetics *11*, 64. 10.1186/s13148-019-0658-5.
93. Goulburn, A.L., Alden, D., Davis, R.P., Micallef, S.J., Ng, E.S., Yu, Q.C., Lim, S.M., Soh, C.L., Elliott, D.A., Hatzistavrou, T., et al. (2011). A targeted NKX2.1 human embryonic stem cell reporter line enables identification of human basal forebrain derivatives. Stem Cells *29*, 462-473. 10.1002/stem.587.
94. Hockemeyer, D., Soldner, F., Cook, E.G., Gao, Q., Mitalipova, M., and Jaenisch, R. (2008). A drug-inducible system for direct reprogramming of human somatic cells to pluripotency. Cell Stem Cell *3*, 346-353. 10.1016/j.stem.2008.08.014.
95. Wu, M., Shang, X., Sun, Y., Wu, J., and Liu, G. (2020). Integrated analysis of lymphocyte infiltration-associated lncRNA for ovarian cancer via TCGA, GTEx and GEO datasets. PeerJ *8*, e8961. 10.7717/peerj.8961.
96. McGinnis, C.S., Murrow, L.M., and Gartner, Z.J. (2019). DoubletFinder: Doublet Detection in Single-Cell RNA Sequencing Data Using Artificial Nearest Neighbors. Cell Syst *8*, 329-337 e324. 10.1016/j.cels.2019.03.003.
97. Wickham, H. (2016). ggplot2: Elegant Graphics for Data Analysis. Springer-Verlag New York.
98. Cao, J., Spielmann, M., Qiu, X., Huang, X., Ibrahim, D.M., Hill, A.J., Zhang, F., Mundlos, S., Christiansen, L., Steemers, F.J., et al. (2019). The single-cell transcriptional landscape of mammalian organogenesis. Nature *566*, 496-502. 10.1038/s41586-019-0969-x.
99. Love, M.I., Huber, W., and Anders, S. (2014). Moderated estimation of fold change and dispersion for RNA-seq data with DESeq2. Genome Biol *15*, 550. 10.1186/s13059-014-0550-8.
100. Supek, F., Bosnjak, M., Skunca, N., and Smuc, T. (2011). REVIGO summarizes and visualizes long lists of gene ontology terms. PLoS One *6*, e21800. 10.1371/journal.pone.0021800.
101. team, R. (2020). RStudio: Integrated Development for R. RStudio. PBC, Boston, MA.
102. Butler, A., Hoffman, P., Smibert, P., Papalexi, E., and Satija, R. (2018). Integrating single-cell transcriptomic data across different conditions, technologies, and species. Nat Biotechnol *36*, 411-420. 10.1038/nbt.4096.
103. Amezquita, R.A., Lun, A.T.L., Becht, E., Carey, V.J., Carpp, L.N., Geistlinger, L., Marini, F., Rue-Albrecht, K., Risso, D., Soneson, C., et al. (2020). Orchestrating single-cell analysis with Bioconductor. Nat Methods *17*, 137-145. 10.1038/s41592-019-0654-x.
104. Street, K., Risso, D., Fletcher, R.B., Das, D., Ngai, J., Yosef, N., Purdom, E., and Dudoit, S. (2018). Slingshot: cell lineage and pseudotime inference for single-cell transcriptomics. BMC Genomics *19*, 477. 10.1186/s12864-018-4772-0.
105. Pantazis, C.B., Yang, A., Lara, E., McDonough, J.A., Blauwendraat, C., Peng, L., Oguro, H., Kanaujiya, J., Zou, J., Sebesta, D., et al. (2022). A reference human induced pluripotent stem cell line for large-scale collaborative studies. Cell Stem Cell *29*, 1685-1702 e1622. 10.1016/j.stem.2022.11.004.

106. Dull, T., Zufferey, R., Kelly, M., Mandel, R.J., Nguyen, M., Trono, D., and Naldini, L. (1998). A third-generation lentivirus vector with a conditional packaging system. J Virol *72*, 8463-8471. 10.1128/JVI.72.11.8463-8471.1998.
107. Longo, P.A., Kavran, J.M., Kim, M.S., and Leahy, D.J. (2013). Transient mammalian cell transfection with polyethylenimine (PEI). Methods Enzymol *529*, 227-240. 10.1016/B978-0-12-418687-3.00018-5.
108. Zhang, Y., Sloan, S.A., Clarke, L.E., Caneda, C., Plaza, C.A., Blumenthal, P.D., Vogel, H., Steinberg, G.K., Edwards, M.S., Li, G., et al. (2016). Purification and Characterization of Progenitor and Mature Human Astrocytes Reveals Transcriptional and Functional Differences with Mouse. Neuron *89*, 37-53. 10.1016/j.neuron.2015.11.013.
109. Mullins, N., Forstner, A.J., O'Connell, K.S., Coombes, B., Coleman, J.R.I., Qiao, Z., Als, T.D., Bigdeli, T.B., Borte, S., Bryois, J., et al. (2021). Genome-wide association study of more than 40,000 bipolar disorder cases provides new insights into the underlying biology. Nat Genet *53*, 817-829. 10.1038/s41588-021-00857-4.
110. Chen, E.Y., Tan, C.M., Kou, Y., Duan, Q., Wang, Z., Meirelles, G.V., Clark, N.R., and Ma'ayan, A. (2013). Enrichr: interactive and collaborative HTML5 gene list enrichment analysis tool. BMC Bioinformatics *14*, 128. 10.1186/1471-2105-14-128.
111. Langfelder, P., and Horvath, S. (2008). WGCNA: an R package for weighted correlation network analysis. BMC Bioinformatics *9*, 559. 10.1186/1471-2105-9-559.
112. Zhang, B., and Horvath, S. (2005). A general framework for weighted gene co-expression network analysis. Stat Appl Genet Mol Biol *4*, Article17. 10.2202/1544-6115.1128.